8-2012

Gain of a Single Gas Electron Multiplier

Mythra Varun Nemallapudi
University of Arkansas, Fayetteville

GAIN OF A SINGLE GAS ELECTRON MULTIPLIER

GAIN OF A SINGLE GAS ELECTRON MULTIPLIER

A thesis submitted in partial fulfillment
of the requirement of the degree of
Master of Science in Physics

By

Mythra Varun Nemallapudi
SASTRA University
Bachelor of Technology in
Electronics and Communication Engineering, 2008

August 2012
University of Arkansas

ABSTRACT

Gas Electron Multiplier (GEM) is a gaseous detector used in particle detection and is known for its high rate capability. Ever since its invention in 1997, GEM was applied in many areas and recently has been proposed to be installed in the CMS high η regions for upgrade at LHC, CERN. A complete understanding of the working and gain behavior does not exist. GEM gain is influenced by charging up and this has been variedly interpreted in literature lacking consensus. I have attempted in this work through simulations and measurements to achieve a better understanding of single GEM gain and how it is affected by various factors. Specific experimental methods which evolved with subsequent measurements were employed to systematically study the charging up effect. Information from simulations was applied to characterize measurements thereby enabling the development of a model for charging up. Conductivity mechanism of the dielectric used in GEM was analyzed and the resistivity measured. Gain free of charging up effects was measured and this is appropriate for comparison with simulations.

[1]

[1] Information presented in this thesis is based on the work that is being published [1]. Overlap of material is hence possible and citation has not been provided at any instance.

This thesis is approved for recommendation
to the Graduate Council.

Thesis Director

Dr. Reeta Vyas

Thesis Committee:

Dr. Hameed Naseem

Dr. William F. Oliver III

Dr. Surendra Singh

Dr. Archana Sharma (*ex officio*)

THESIS DUPLICATION RELEASE

I hereby authorize the University of Arkansas Libraries to duplicate this thesis when needed for research and/or scholarship.

Agreed _____

Mythra Varun Nemallapudi

Refused _____

Mythra Varun Nemallapudi

ACKNOWLEDGEMENTS

This work would not have been possible without the kindness of few people who I would like to thank.

I wish to express my gratitude to Dr. Archana Sharma for providing me an invaluable opportunity to work at CERN, for offering me the necessary financial support, and for inspiring me in many ways. My sincerest thanks to Dr. Rob Veenhof for his invaluable guidance and mentoring with the project as my supervisor.

I thank Dr. Leszek Ropelewski for his mentoring and for permitting me to use the RD-51 laboratory at CERN. A special thanks to Sven Dildick for the training he offered so kindly at the start of the project. I thank Laura Franconi for introducing me to the RD-51 lab and for being patient while helping me with some tricky measurements. I would like to thank Dr. Renju Thomas, Marco Villa, Michal Zientek, Özkan Şahin, Yalçın Kalkan, Ankit Mohapatra and other colleagues at CERN for their thought provoking discussions. A special thanks to Andrey Marinov and Stefano Colafranceschi for being great mentors at the lab. Thanks to Miranda van Stenis for patiently fabricating experimental apparatus that was often customized.

I would like to thank Dr. Reeta Vyas for advising me and helping me with the planning and execution of my thesis and defense. I thank the Department of Physics at University of Arkansas for the financial support.

Special thanks to my friend Vikash Kumar Mishra for being a constant source of support and inspiration. I am deeply indebted to my family and friends for their unconditional love and support that gets me going.

DEDICATION

"sarvāṇīndriya-karmāṇi prāṇakarmāṇi cāparē |

ātmasaṁyamayōgānau juhvati jñānadīpitē ||"

— Chapter 4, Verse 27, Srimad Bhagavat Gita

Translation: Others offer the actions of their senses and vital breath, to the fire of knowledge of a controlled mind.

CONTENTS

LIST OF FIGURES

LIST OF TABLES

1 INTRODUCTION

Gas Electron Multiplier (GEM) is a detector employed in High Energy Physics for particle detection and has been invented in 1997 by Fabio Sauli at CERN [2]. GEM operation is based on avalanche multiplication in a gas medium effectively achieving amplification of the originally ionized charges. GEMs belong to a class of detectors namely MicroPattern Gas Detectors. These are the newer generation of detectors.

Objective — This work was devoted to understand the gain of a CERN standard single GEM through simulation and experiments. Penning effect has been included to make the simulations accurate. GEM simulations have been performed in the parameter space with a special emphasis on obtaining the penning parameter by fitting with the experimental data. Experimental measurements have been taken for this purpose. Influence of charging up on gain was studied through systematic measurements. Polyimide conductivity mechanism was experimentally studied in detail.

1.1 Topology of the research work

The research work was performed at CERN as a part of the collaboration 'GEMs for CMS,' constituted to propose the installation of GEMs for the high eta upgrade of Compact Muon Solenoid (CMS) experiment, which in turn is one of the major experiments at the Large Hadron Collider (LHC) located at the European Center for Nuclear Research (CERN). A brief description of each element of the hierarchal structure has been provided below to provide the context and topology of the research work that was performed. This work is limited to a single GEM which is the basic version of a GEM. GEMs that were proposed for CMS application are three stage versions of a single GEM, termed as 'triple-GEMs.'

CERN CERN is among the best laboratories of the world engaged in scientific research of highest order. Work at CERN is directly or indirectly related to fundamental physics and

constant efforts are directed to unravel the mysteries of nature by creating conditions where the building blocks of nature and their interactions can be observed. It houses the biggest particle accelerator LHC.

LHC LHC is the world's largest particle accelerator located at CERN. It was designed to operate at a center of mass energy of 14 TeV and a luminosity of 10^{34} $cm^{-2}.s^{-1}$. It is a 27 km long circular tunnel passing through the Swiss and French borders and is located underground at an average depth of 100 m. Nuclei are accelerated over a series of steps through electric fields in order to reach speeds close to the speed of light. Directional control over the nucleons is obtained by applying magnetic fields generated by dipole magnets located along the tunnel. Opposing particle beams are accelerated to prepare them for collision at specific points called as the interaction points. At these locations where particle collisions occur, the incident particles are shattered giving rise to a myriad of subatomic particles. Since microscopes cannot be used to observe such particles whose sizes are well below the wavelength of light, specific detectors are designed for this purpose. Below is a list of such detector experiments.

- A Toroidal LHC Apparatus (ATLAS)
- Compact Muon Solenoid (CMS)
- A Large Ion Collider Experiment (ALICE)
- Large Hadron Collider beauty (LHCb)
- TOTal Elastic and diffractive cross section Measurement
- Large Hadron Collider forward (LHCf)

CMS Compact Muon Solenoid is one of the two general purpose detectors at CERN (the other being ATLAS) with 'discovery of Higgs boson' being one of the principal objectives

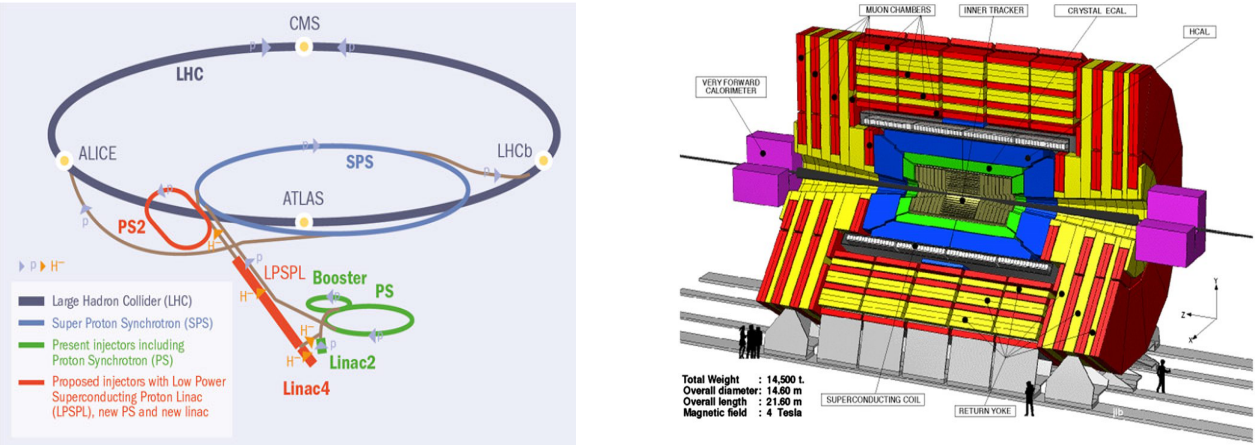

Figure 1.1: Left: Schematic of the LHC [3], Right: Schematic of CMS [4]

that can help understand the electroweak symmetry breaking. Incidentally, the discovery of a particle with properties similar to a Higgs boson was recently confirmed by CERN. A solid iron code magnet is used to supply the magnetic field which is of the order 4T. In order to have a comprehensive evidence for the discovery of Higgs particle, the results from CMS are expected to be consistent with the results from ATLAS. CMS has various detectors arranged in layers similar to cylindrical onion structure with each layer having a different functionality. The inner regions of the detector under the influence of the magnetic field are used to track charged particles. Layers in between form the calorimeter to detect photons and hadrons. Outermost layers are designed for the detection of muons, particles which escape detection and decay in the prior regions. CMS is a hermetic detector meaning that it can detect particles leaving in every direction except the ones that travel inside the beam pipe. For a more comprehensive understanding of CMS refer to the technical design report [5].

Gas Electron Multipliers for CMS As a part of CMS is 'GEMs for CMS', a research collaboration which has proposed GEM detectors to be installed in specific regions of the CMS experiment which are prone to high particle rates. The proposal comes in view of the high rate capability and radiation resistance of GEMs. My research work at CERN was performed as a part of this collaboration.

1.2 Context of the project in relation to CMS

LHC will stop operating for the the long shutdown (LS2) in the year 2013 for maintenance and up-gradation. Prior to the shutdown LHC operates with a beam energy of 4 TeV, post shutdown it will eventually operate with a beam energy of 7 TeV. During this shutdown it has been proposed that the high pseudo-rapidity (η) regions of the CMS should be instrumented with triple GEMs. Pseudo-rapidity has been defined according to eq 1.1. Where θ the angle made by the momentum vector of the high energy particle with the beam axis.

$$\eta = -ln\left[tan\left(\frac{\theta}{2}\right)\right] \tag{1.1}$$

Currently the regions of CMS with $|\eta| > 1.6$ are vacant in spite of the original proposal to instrument them with Resistive Plate Chambers (RPC). Post LS2 the conditions are expected to be hostile for the detectors due to a higher luminosity especially in the high η region.

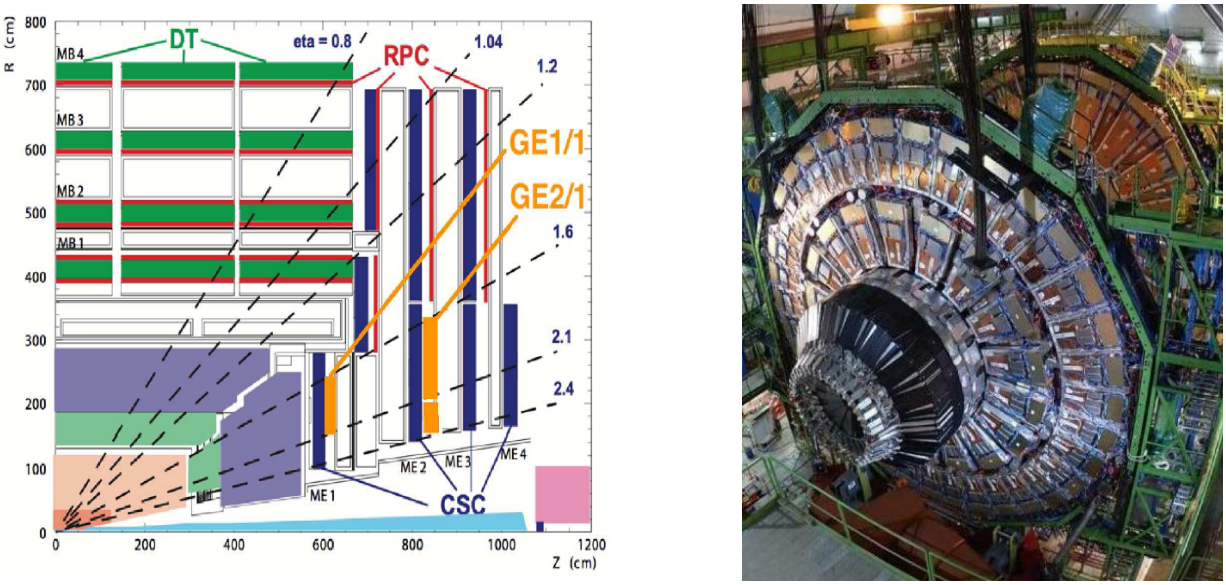

Figure 1.2: Left: Transverse view of the CMS muon trigger and tracking sections. Right:CMS Endcap YE1 disk with high η region (nose) [5]

Fig 1.3 shows the regions of the CMS end caps where the GEM detectors will be installed. Presently the muon detection in CMS is achieved through Cathode Strip Chambers (CSC)

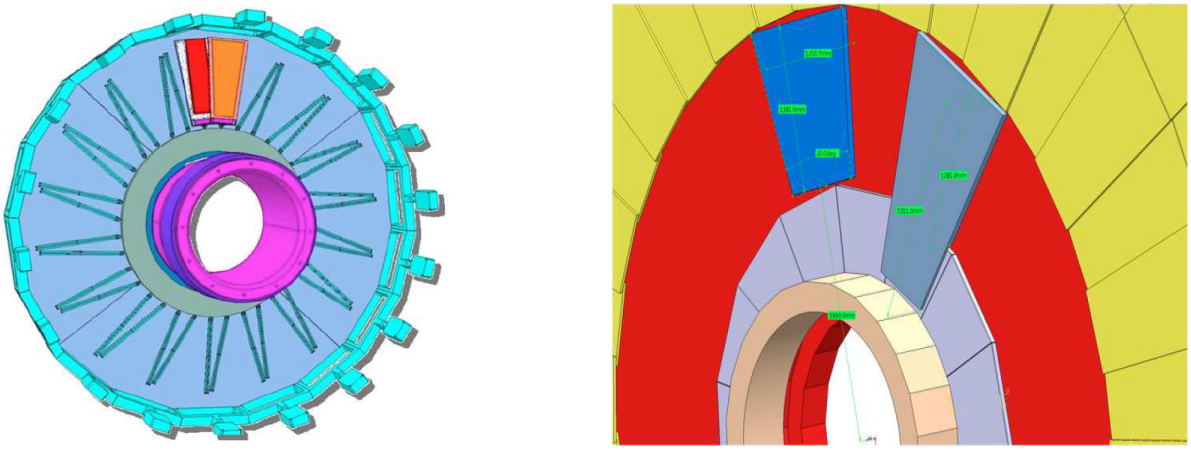

Figure 1.3: CMS endcap structures for the GE1/1 chamber (left) which is mounted on the YE1 nose and GE2/1 chamber (right) which will be mounted behind the YE1 [5]

and Resistive Plate Chambers (RPC) as seen in fig 1.2. Drift Tubes (DT) are used in the low eta regions where the neutron background is extremely small. While RPCs are designed to operate under rates of the order 100 kHz/cm^2, CSCs are employed in the regions with higher rates. However, CSCs are bound to be deteriorate over time due to the intense operating rates expected. This will pose a problem to the fundamental design philosophy of CMS which is to have a redundant muon system especially in the regions $1.6 < |\eta| < 2.4$

In view of the magnitude of GEM's usage it is imperative to develop a complete understanding of the physics of GEM gain and operation. This understanding can be developed through simulations and experiments which directly offer insights into the physical processes at work.

1.3 Gas detectors

GEMs belong to the class of detectors called gas detectors which work on the principle of avalanche multiplication in gas medium under the influence of electric fields.

When a high energy particle enters a gas medium, it deposits energy through interaction with the atoms and molecules of the gas. The Bethe Bloch equation describes the process of energy loss of an incoming charged high energy particle which occurs due to the particle's

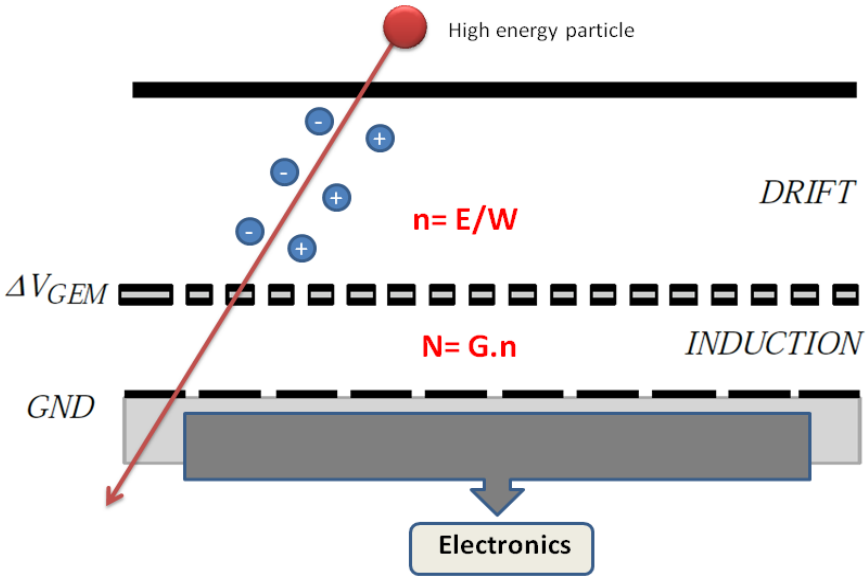

Figure 1.4: Charge creation and multiplication inside a GEM detector. The amplification stage lies between drift and induction gaps.

electromagnetic interaction with the gas atoms [6]. If an Xray photon of energy E is used as the incident ionizing radiation for a gas medium with work function W, the number of charge pairs created is given by the following eq 1.2. This process is subject to statistical fluctuations and hence has a Poissonian distribution with the mean and variance described in eq 1.2.

$$\mu(n) = \frac{E_\gamma}{W_{\text{gas}}} \; ; \; \sigma(n) = \sqrt{F.\mu(n)} \tag{1.2}$$

Where 'F' is the fano factor, which arises because the nature of ionizations is not purely statistical [7]. Individual cases of charge creation cannot be treated independently because of the existence of energy levels. The existence of Fano factor improves the energy resolution of a particle detector. Fano factor for Ar is ~ 0.2.

The number of primary charges created is too small to be detected by the electronics. An amplification stage (see fig 1.4) is introduced to achieve charge multiplication. The factor by which the initial number of charges are multiplied is termed as gain 'G.' These charges eventually drift towards the readout plane and the signal is read by the electronics.

The increase in the number of electrons brought by the amplification depends on the

Townsend coefficient (α) and is proportional to the initial number of electrons and the incremental distance as shown in eq 1.3.

$$dN = N\alpha dx \tag{1.3}$$

To estimate the final number of electrons, the above equation is integrated over the entire path where the field concentration is high.

$$N = N_0 \exp \int \alpha dx \tag{1.4}$$

For a more comprehensive theoretical treatment of gas detectors consult [8].

The following paragraphs provide a brief description of the evolution of the gas detectors.

1.3.1 Proportional Counter (PC)

Proportional counter consists of an anode wire with a high voltage supply surrounded by a cathode cylinder. Electrons created from the ionizations drift towards the anode under the influence of electric fields. Near the regions close to the wire, high fields cause a Townsend avalanche giving rise to a signal. This signal energy will be proportional to the energy of incident ionizing radiation when the detector is operated in the proportional region as shown in fig 1.5 When the voltage of anode wire is appropriately chosen it works in a proportional region. For low voltages, there is no amplification. For higher voltages, the space charge effect becomes dominant. Production of electron ion pairs causes the accumulation of slow moving ions to form a positive ion cloud. This distorts the electric field and results in a deviation from proportionality. Even higher voltages result in a discharge like phenomenon which is independent of the incident radiation's energy. This region is called the Geiger-Muller region.

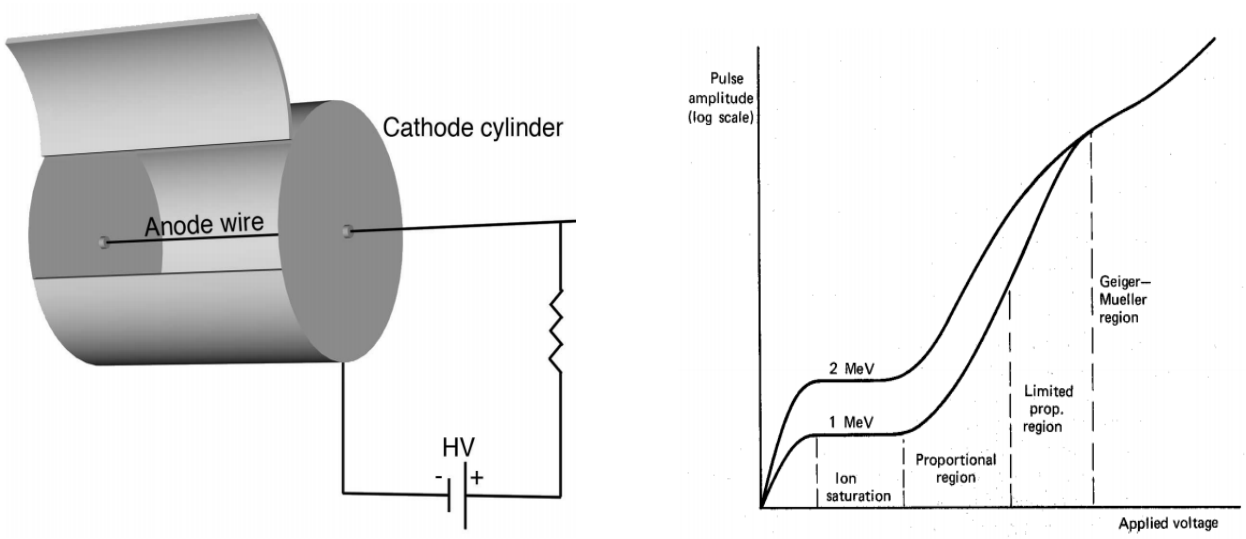

Figure 1.5: Left: Schematic of a PC; Right: Operating regions of gaseous detectors [9]

1.3.2 Multi Wire Proportional Chamber (MWPC)

These detectors are proportional counters with position sensing capability. MWPC was invented by Georges Charpak and collaborators in 1968 [10]. The electric fields close to the wire are extremely high and cause avalanche breakdown when a charge ventures.

Anode wires are parallel resulting in a field configuration as shown. All anode wires are maintained at a same potential and are sandwiched between cathode planes. Charges created by the ionization particle, drift along the field lines to move closer to the anode wires. Avalanche generation occurs at regions very close to the wire. The position of the incident particle can be identified by locating the wire on which the signal has been induced. Signal will be highest on the wire which is nearest to the position of the ionizing radiation. The spacing between the wires affects the position resolution. There exists a capacitive coupling between the wires which induces a negative signal. The positive ions created from the avalanche generation move towards the anode wires compensating the signal from capacitive coupling.

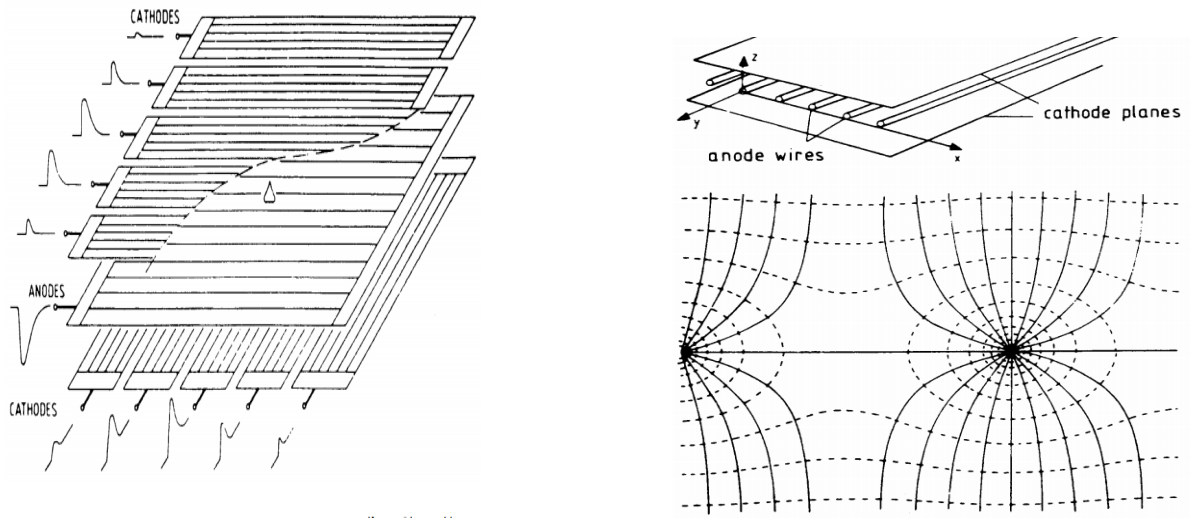

Figure 1.6: Left: Schematic of a MWPC; Right: Cathode plane segmentation for better position sensing [9]

1.3.3 Drift Chamber (DC)

A drift chamber is a modification of MWPC with an enhanced spatial resolution. Charge created by incoming ionization takes a finite amount of time to drift towards the anode wire and induce the signal through an avalanche. This transit time of the charge is dependent on its initial position. Using this timing information, the position can be evaluated. The wire anode spacing is higher than in a MWPC. They have achievable position resolutions of ~ 100 μm

1.3.4 Micro Strip Gas Chambers

MSGCs were a development of wire chambers to overcome the limitation on wire gap through microelectronics fabrication techniques. Strips of metal deposited on a substrate act as the anode. The cathode plane is located around 60 μm from the anode strips. This enables the positive ions to reach the cathode much faster thereby avoiding the formation of charge clouds which lead to a space charge effect thereby enhancing rate capability. Strip gaps of around 200 μm can be created which result in a finer resolution.

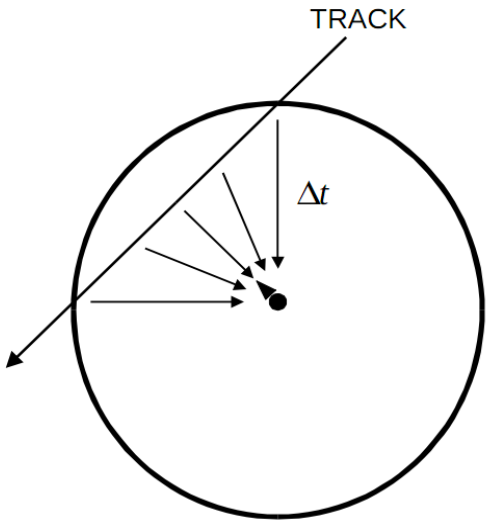

Figure 1.7: Ionization track in a drift chamber[11]

Problems with MSGCs have been identified due to discharge-induced damages of the detector. High voltage working conditions and high rates of operation cause discharges which completely render the anode strips unusable. Example of this can be seen in the fig 1.8.

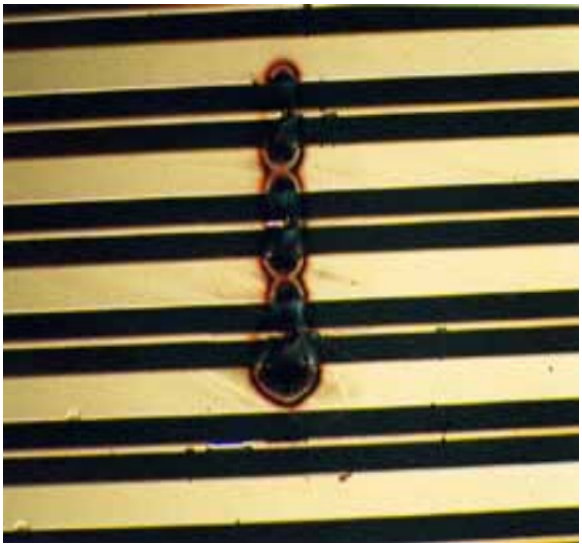

Figure 1.8: Discharge induced damage on a strip of MSGC [12]

1.3.5 Micro Pattern Gas Detectors (MPGD)

Development of MPGDs was a solution for most of the aforementioned problems. Employment of microelectronics in the fabrication of detectors has given rise to a number of possibilities in the designs which were not practical before. Thin anode strips vulnerable to discharges are replaced by thicker metal structures which can resist discharges better. They also have a higher rate capability and better reduction of photon feedback. Usage of polyimide and glass substrates, employment of photo-lithographic techniques to etch the substrates and employment of printed circuit boards have contributed to the development of MPGDs. Listed below are some of the current technologies of MPGD-

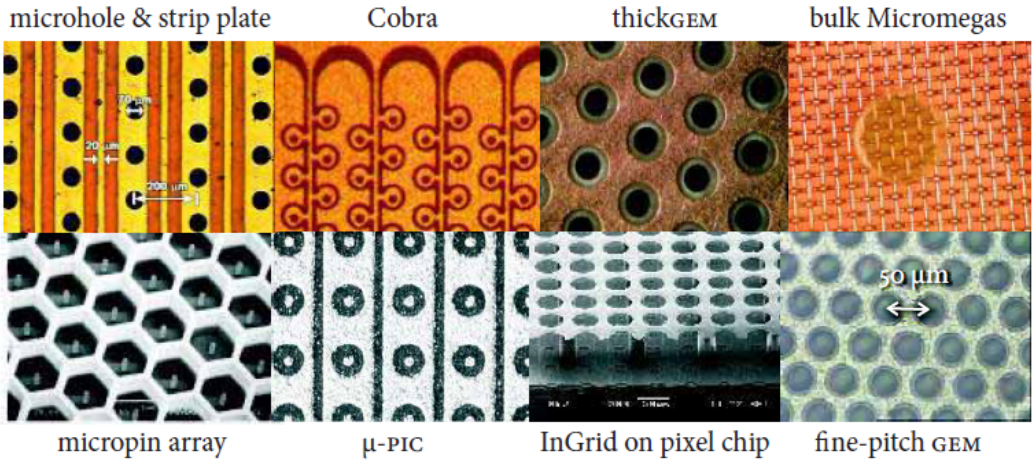

Figure 1.9: Current technologies of MPGDs [12]

Single GEM Single GEM is a planar dielectric clad in metal with holes etched through the metals and the dielectric. It is an amplification structure which is independent of the readout. Detailed study of the GEM structure and working will be dealt along this thesis. Multiple layers of GEM can give rise to further amplification. The dielectric used is a polyimide with a thickness of the order 50 μm. Copper layer of 5 μm thickness is deposited on either surface. Through photo-lithography and etching techniques holes are etched through

the layers of the GEM. Due to limitations of chemical etching techniques and the size of the holes to be etched, a uniform cylindrical hole cannot be achieved.

Triple GEM Triple GEM has three single GEMs cascaded to give rise to an enhanced amplification. This is the common model used for practical applications. A separate HV divider circuit enables the voltage distribution to the GEM metals of various stages.

NS2 This is a self stretching technology developed in the CERN lab by Rui Oliveria [13]. In NS2 technique the usage of a frame and gluing are avoided. Foil is fabricated with a pattern of holes on the edges. These holes can directly be placed into the detector unit fitting into the alignment pins. Stretching is then performed mechanically. NS2 triple GEM with 30 mm $\times$ 30 mm dimensions has been tested in the RD-51 laboratory.

2 GEM WORKING

2.1 Structure of a single GEM

GEM comprises a thin sheet of dielectric material with metal coating on either side. This structure has an array of staggered hexagonal holes through the two metals and the dielectric fabricated via an etching technique [2]. Limitations in the etching procedures and the geometric constraints result in a bi-conical hole. Fig 2.1 gives a view of GEM.

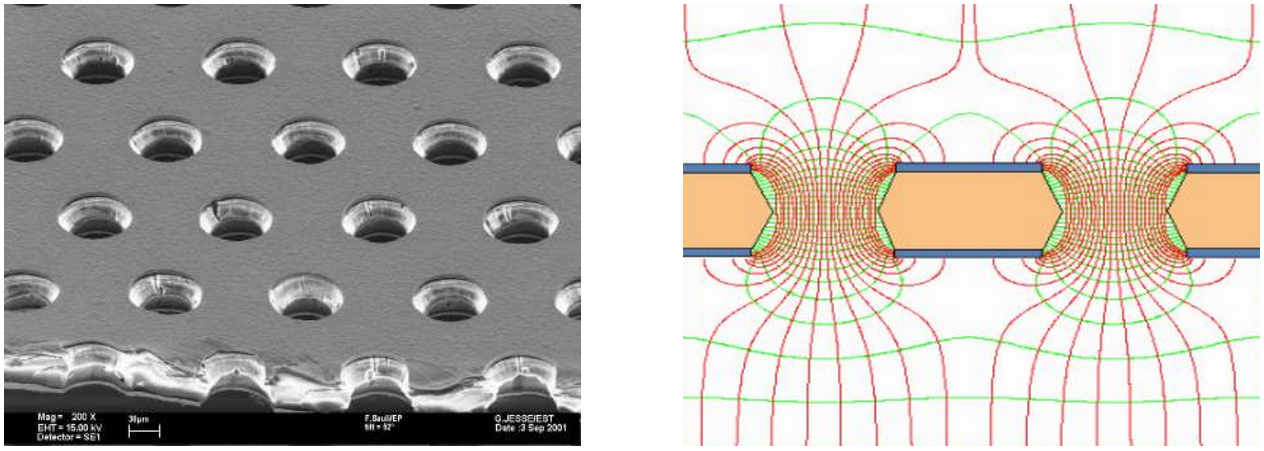

Figure 2.1: Left: Microscopic image of a GEM, Right: Cross sectional view showing the metal layers and polyimide. The field lines are shown to represent the concentration of electric field inside the hole and near the metal edges [14]. The biconical shape of GEM hole can also be seen.

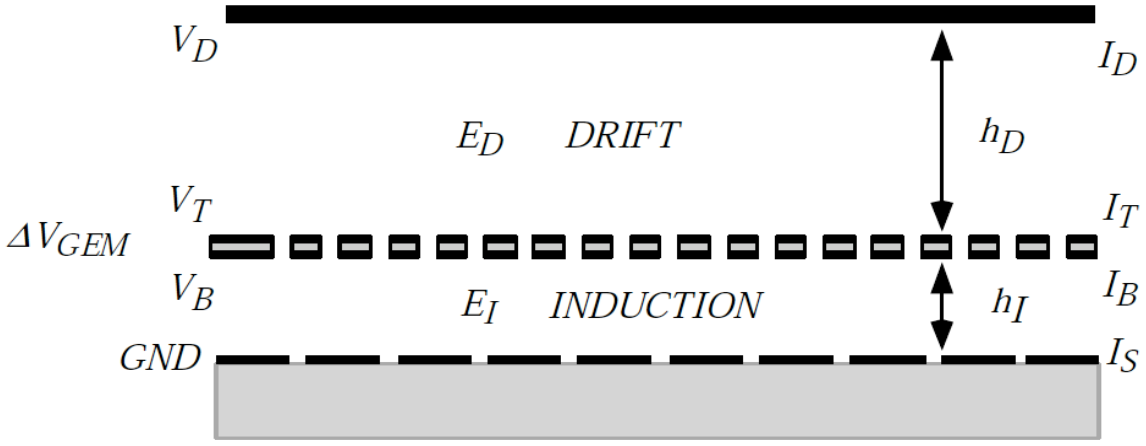

Figure 2.2: Schematic of a single GEM [14]

Fig 2.2 describes the schematic of a GEM under operation. The topmost plane is the drift plane which is maintained at a potential V_{D}. GEM is located below the drift plane where V_{T} and V_{B} are the potentials at which the top and bottom metals are maintained respectively. Readout is performed by metal strips on a printed circuit board which is located below the GEM (see fig 1.4). The gaps above and below GEM plane are drift and induction gaps respectively. Current on the drift plane is I_{D}, top metal is I_{T}, bottom metal is I_{B} and readout plane is I_{S} (signal current). For all measurements performed in the context of this thesis, only the signal current has been measured.

Parameter	**Value**
Area (cm^2)	10x10
Metal thickness (μm)	5
Polyimide thickness (μm)	50
Out-dia (μm)	70
Inner-dia (μm)	50
Pitch (μm)	140
Drift gap (mm)	3
Induction gap (mm)	2

Table 2.1: Specifications of a CERN standard single GEM

2.2 Operational Parameters

Listed below are some of the parameters of the GEM and other terms frequently used throughout the thesis.

- Top metal— The metal layer of a GEM to which lower potential is applied and is closer to the drift plane.
- Bottom metal— The metal layer of a GEM to which higher potential is applied and is closer to the induction plane.
- Metal thickness— Thickness of the metal surfaces of the GEM.
- GEM hole— Hole from top metal to bottom metal through the dielectric.

- Out-dia— Diameter of the GEM hole at the entrance and exit hole on the metal surface.
- Inner-dia— Diameter of the GEM hole halfway between entrance and exit holes at the waist region of the bi-conical section.
- Pitch— Pitch is the distance between the centers of adjacent GEM holes.
- Drift plane, field and gap— Drift plane is the topmost plane of a GEM detector which is a metal sheet with the lowest potential and acts as a cathode in order to provide the drift field across itself and the top metal of a GEM. The region enclosed between the drift plane and top metal is the drift space where the primary charges are produced in an ionizing track caused by the incident ionizing radiation.
- Induction plane, field and gap— Induction plane is the bottommost plane of a GEM detector which is a metal plane with the highest potential and acts as the anode in order to attract the electrons created as a result of avalanche near the GEM hole. Induction plane is usually maintained at ground potential. The region enclosed between bottom metal and induction plane is the induction gap.
- Total gain— The total number of electrons created in a GEM per incident primary charge inclusive of the charges lost by various means.
- Effective gain or gain— The net charges reaching the anode plane in a GEM per incident primary charge exclusive of losses.
- Optical transparency— Ratio of the total area of holes to the area of metal in a GEM metal. This ratio determines the degree of ease with which a normally incident electron can freely pass through the GEM under the absence of any applied fields.
- Primary charge— Charge generated due to ionization caused by the incident radiation.
- Secondary charge— Charge that results from the avalanche multiplication of the primary charge under the influence of the applied electric field.

2.3 Electric field

Electric field is applied in a GEM detector for (a) drifting the charges steadily towards the anode, and (b) supplying charges with energy to cause further ionizations to lead to avalanche multiplication.

Drift field (E_{D})- Electric field created in the drift space which causes the primary charges to move towards the GEM. This field depends on the potential difference between GEM top metal and the drift plane, and the drift gap.

Amplification field- Inside the GEM hole, the electric field is between 50 and 100 times the drift field depending on the latter and the applied voltage across the GEM metals. As a result the field is large enough to cause a rapid gain in the electron energy leading to avalanche multiplication. This field is dependent on the voltage difference between the top and bottom GEM metals, and the thickness of the dielectric.

Induction field (E_{I})- Electric field created in the induction gap which causes the charges created in the avalanche to move towards anode plane. This field depends on the potential difference between the anode ground and GEM bottom metal, and the induction gap.

2.4 Gas mixture

GEM works in a gas medium where the electrons accelerating under the influence of electric field ionize the gas atoms to further create charges forming an avalanche. The standard operational gas mixture for the GEM is $\mathrm{Ar} - \mathrm{CO}_2$ mixed in a 70/30 ratio. Although this is the dominant composition used for this work, various percentages of the standard gases have been used in our studies. In a purely Ar based medium, avalanche multiplication can often occur beyond limits. This generates a massive number of charges that rain down the detector causing sparks. Such sparks can permanently damage the detector and are hence

undesired. CO_2 functions as a quencher gas in this medium. Due to the electro-negativity of CO_2, it attracts the electrons which get attached to the CO_2 molecule. This effectively keeps a check on the size of the avalanche. CO_2 also gives rise to penning effect which will be discussed in a greater detail in section 3.2.

2.5 Avalanche multiplication and amplification

Primary charge drifts towards the GEM top metal under the influence of the drift field. When the primary charge gains energy rapidly under the influence of the electric fields inside a GEM hole, its interaction with the gas medium results in an occasional ionization when the electron attains an energy higher than the ionization potential of the gas mixture. A charge that is created by a primary charge which is also under the influence of electric field gain energy as it moves. Similar to a primary charge, it can further create ionizations depending on its energy. This process continues like a chain reaction as long as the electrons have energies above the ionization threshold supplied by the electric field. The multiplication of the number of charges from the initial charge is termed as avalanche multiplication.

3 THEORY

3.1 Avalanche statistics

Ionizing radiation generates a certain number of primary electrons in the drift gap of the GEM. This number will be multiplied by the amplification factor G to get the final number of charges reaching the anode. Due to the statistical nature of the electron multiplication process the gain has a probability distribution with a mean and variance. Avalanche size is the total number of electrons generated from the initial charges due to avalanche multiplication. Let us consider a single electron that gives rise to n electrons due to avalanche multiplication. The electron can undergo any kind of multiplication giving rise to the final number of electrons. It may undergo a very large multiplication or not multiply at all. Since the number n is variable, the most probable outcome will be none and the higher avalanche sizes will be progressively less probable. The probability to have a certain final number of electrons will be a normalized exponential distribution with a mean G as shown in eq 3.1.

$$G(n) = \frac{1}{G} e^{\frac{-n}{G}} \tag{3.1}$$

Consider the case of 2 electrons to begin with. They undergo avalanche multiplication to give rise to n electrons eventually. The contribution from each of the two electrons can be varied. Considering that the first electron gives rise to an avalanche of size x, the second electron contribution will be $n - x$. x is an arbitrary number that can be anything between 0 and n. This can be represented through the following equation.

$$G(n) = \int_0^n P(x) \times P(n - x) \mathrm{d}x \tag{3.2}$$

$P(x)$ and $P(n-x)$ are the contributions of the first and second electrons, respectively, to the avalanche. The values can be substituted and solved in the following manner.

$$G(n) = \int_0^n \frac{1}{G} e^{\frac{-x}{G}} \frac{1}{G} e^{\frac{-(n-x)}{G}} \mathrm{d}x$$

$$G_2(n) = \frac{n}{G^2} e^{\frac{-n}{G}} \tag{3.3}$$

In a similar manner the probability distribution for the avalanche size with 3 initial electrons can be calculated as shown in eq 3.4

$$G_3(n) = \frac{n^2}{G^3} e^{\frac{-n}{G}} \tag{3.4}$$

Extrapolating this result to an arbitrary number of primary charges r, we get the following distribution.

$$G_r(n) = \frac{n^{r-1}}{G^r} e^{\frac{-n}{G}} \tag{3.5}$$

The polynomial term dominates the behavior of the curve near $n = 0$ and causes a steep rise with higher powers. The exponential term dominates in the higher values of n suppressing the rise caused by polynomial and eventually brings down to zero. The resulting distributions are gamma functions. When r in eq 3.5 assumes higher values, the function takes a Gaussian distribution according to the central limit theorem [15].

3.2 Penning effect

In a gas mixture where an ionizing radiation is incident, the input energy can be utilized in both ionizations and excitations depending on the interaction cross sections. Ordinarily the energy from excitations is lost in the form of a radiative or non-radiative transfer. However, if the excited state of one gas atom is higher than the ionization potential of another gas present in the mixture, an excited state in the former gas atom, with some probability, can give rise to an ionization in the latter. This kind of a transfer is called as a 'Penning

transfer' named after Frans Michel Penning [16]. In relation to gas detectors, which work on the principle of avalanche multiplication inside the gas medium, the penning effect enhances the multiplication from the usual amount by converting the otherwise lost excitations into ionizations which release a free electron. This results in an increased gas gain.

The electronic configuration of ground state and excited states of Ar are listed below in the increasing order of energy.

- Ground state — $1s^2\ 2s^2\ 2p^6\ 3s^2\ 3p^6$
- 1^{st} excited — $1s^2\ 2s^2\ 2p^6\ 3s^2\ 3p^5\ 4s$ (< 11.83 eV)
- 2^{nd} excited — $1s^2\ 2s^2\ 2p^6\ 3s^2\ 3p^5\ 4p$ (13 eV)
- 3^{rd} excited — $1s^2\ 2s^2\ 2p^6\ 3s^2\ 3p^5\ 3d$ (13.85 eV)

The ionization energy of CO_2 (13.77 eV) lies between the 2^{nd} and 3^{rd} excited states of Ar. The excited atom Ar^* with an electron in the 3d state causes a penning transfer resulting in the ionization of a CO_2 atom by collision. Excited atom Ar^* is highly reactive and behaves similar to an alkali metal due to a single electron present in the outermost shell [17].

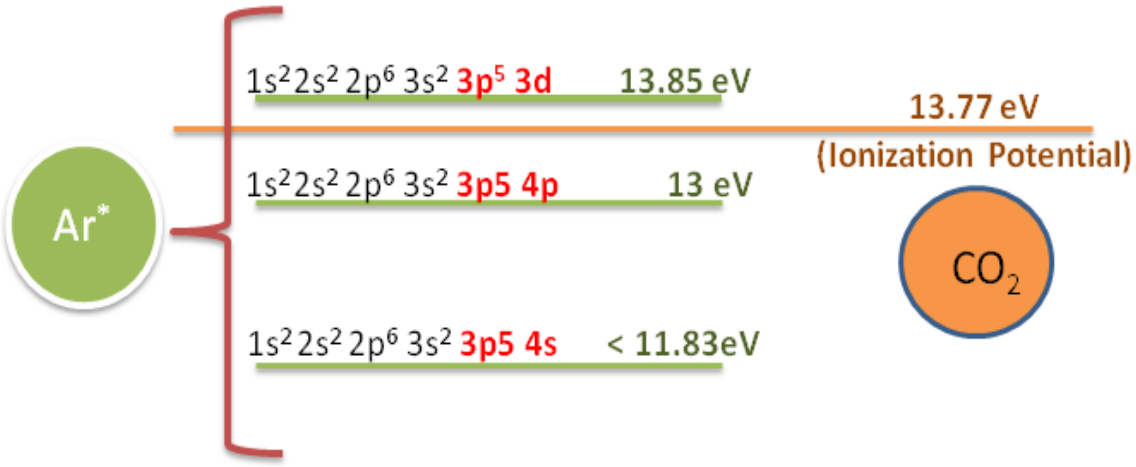

Figure 3.1: Excitation levels of Ar atom in comparison with the ionization potential of CO_2

$$Ar^* + CO_2 \rightarrow Ar + CO_2^+ + e^- \tag{3.6}$$

There are multiple ways in which such a transfer is possible-

Direct transfer The outermost e^- in the Ar^* undergoes a radiative transfer releasing a photon. This photon is absorbed by the CO_2 which gets ionized releasing an electron.

Indirect transfer This process is akin to the Auger emission process. An electron tunnels from the CO_2 and kicks out the electron from the outer shell of Ar^*.

Due to the inclusion of Penning effect, the Townsend coefficient is redefined according to eq 3.7

$$\alpha_{\text{eff}} = \alpha \left(1 + r\frac{\nu_{\text{exc}}}{\nu_{\text{ion}}}\right) \tag{3.7}$$

A study on penning transfers in various gas mixtures can be found in [17].

3.3 X-ray

In the real operation of detector, high energy particles such as muons are a source of ionizing radiation while the measurements in the lab are performed using X-rays as source. Understanding the X-ray production mechanism is essential to study the effects it has on the pulse height spectrum, which will be discussed in section 5.2.

The X-ray tube has a copper target and gives rise to X-ray photons K_α and K_β with respective energies of 8.0 keV and 8.9 keV. The mechanism behind the X-ray generation is depicted in the fig 3.2.

A thermally heated tungsten filament at the cathode emits electrons. A copper target acts as anode setting up an electric field in which the electrons accelerate. The voltage in the X-ray tube can be externally adjusted and a setting of 10 kV will impart 10 keV energy to the electron with which it hits the target. This causes the electrons in the K shell of Cu to get excited and de-excited emitting radiation in the process (see fig 3.3). When the de-excitation happens from L shell it is called K_α and from M shell it is called K_β.

The movement of electrons close to the nuclei causes them to loose energy in the form

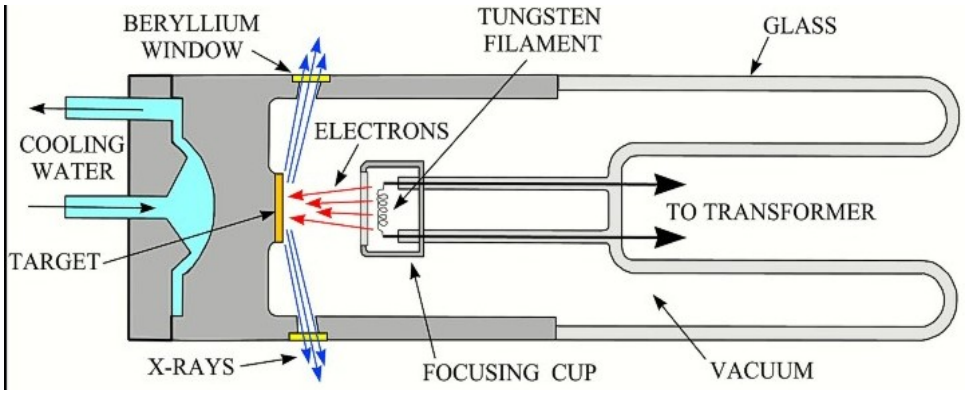

Figure 3.2: Schematic for Xray generation [18]

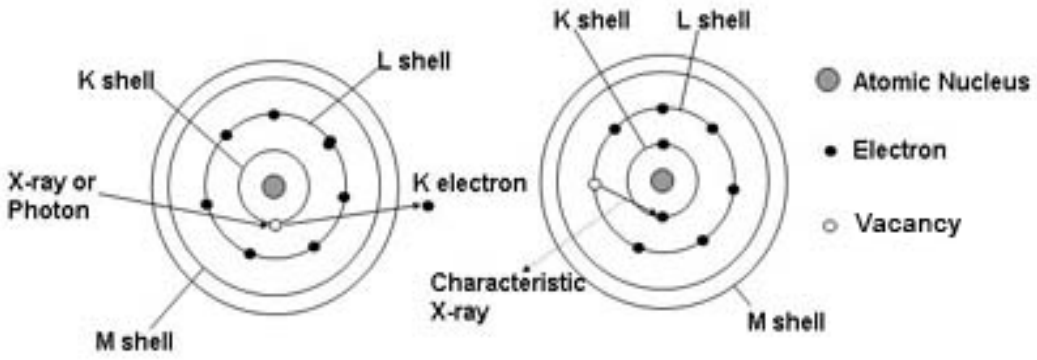

Figure 3.3: Electron transitions betweens shells of a Cu atom causing Xray generation [19]

of undesired radiation and this is termed as Bremsstrahlung literally meaning 'breaking radiation'.

When the X-rays interact with the gas medium of Ar and CO_2 they are absorbed by the Ar atoms where every photon transfers the entire energy to a single electron. Photo absorption can cause excitations or ionizations. Ionizations contribute to the photo peak of the Pulse Height Spectrum. The cross section of Argon is at 3.21 eV while it has excitation levels from K shell at 3.19 eV and 3.2 eV. Hence these transitions during the de-excitation result in radiations that are lost without contributing to the gain. This contributes to an escape peak in the pulse height spectrum.

4 SIMULATION OF GAS GAIN

Monte-Carlo simulations with computer programs and other software packages were performed to understand the performance of a GEM in its parameter space. Although experimental data for GEM has been available, a complete physical understanding of the working was not achieved. Through electron microscopic tracking, this understanding is more complete due to the inclusion of penning transfer.

4.1 Software

ANSYS ® ANSYS [20] is a commercially available finite element method (FEM) software that is used to design the geometry and create maps of electric field. Through scripting a model of GEM was constructed and a unit cell which is a basic repetitive structure. Parameters for the ANSYS model are the same as the CERN standard single GEM. The unit cell also includes drift and induction gaps where charge transport occurs. Second order tetrahedral elements with parabolic faces were used for the calculations. The resulting electric field maps are stored in *.lis* files. These maps contain the electric field information at every point inside the defined GEM geometry.

Magboltz Magboltz [21] is a program which employs Monte-Carlo technique to solve the electron transport equations in a gas medium. It contains the interaction cross sections for various gases. Since GEM works in a gas medium, the avalanche generation due to charges moving in the gas depends on the interactions the electrons have with the gas atoms.

Garfield++ Garfield++ [22] is a program developed to simulate particle detectors. In the present context, a gas medium is used although it can also be applied to semiconductor media. The program is interfaced to ANSYS for field maps and Magboltz for calculating the electron transport parameters. Interface with Heed can help realize the charged tracks created by an incident ionizing particle. The newer version encapsulates electron transport

with penning transfer taken into account.

4.2 Simulation method

GEM geometric model has been constructed using ANSYS. The standard settings for the simulation have been listed in table 4.1. The specifications of the GEM are chosen according to CERN standard 10 cm $\times$ 10 cm single GEM as listed in table 2.1. Depending on the aim of the simulation, one or more parameters will be varied to observe their dependence on the behavior. The operational gas mixture is $Ar - CO_2$ with the standard ratio of 70/30.

Parameter	**Value**
Drift field ($V.cm^{-1}$)	2000
Induction field ($V.cm^{-1}$)	3000
ΔV_{GEM} (V)	300-500

Table 4.1: Parameter settings for simulation

The ANSYS simulation generates electric field maps that are store in the files PRNSOL.lis, ELIST.lis, MPLIST.lis, NLIST.lis. These will be read by the Garfield++ script which interfaces it with Magboltz.

Each simulation is performed for a single electron entering the drift space from a random location along the top plane. The electron will be subsequently tracked at every step by the program. Ionizations produced in the process will be stacked and dealt sequentially after completely tracking the initial electron upto the end of Induction gap.

Occasionally the simulation generates avalanches of extremely large sizes. These consume immense memory to process, thereby leading to the job crash. In order to avoid this, limit has been placed on the avalanche size through a modification in the script and the source code.

4.3 Gas gain of standard GEM

Gain is defined as the average number of electrons reaching the anode per primary electron. For the simulation purpose, the number of electrons reaching 50 μm below the bottom metal plane of the GEM has been considered for computing gain. Gain varies with almost every parameter involved in the operation of a GEM. These include electric field, gas mixture, GEM-geometry, metal thickness etc. Simulations have been performed to identify the ideal range of parameters in the region of operation. This main idea was to simulate the gain to match the experimental data.

4.4 Effect of gem hole diameter

GEM gain dependence on hole diameter has been experimentally studied by Sebastian et al. in [14]. It has been found that the gain is low for higher values of diameter and increases with decreasing hole diameter. Optimal value was reportedly reached for the value of hole diameter close to the thickness of polyimide. For lower values of hole diameter, the gain lay on a plateau region indicating a stable operating region. This has been cited as a guaranteeing factor for GEM performance in spite of the inconsistencies in the hole diameter due to manufacturing limitations.

In order to understand the variation of GEM gain with the hole diameter through simulation, the ratio of outer to inner diameter has been kept a constant at 1.4. The effect of diameter on gain can be seen from the plot 4.2. GEM outer diameter was varied with $E_{\mathrm{D}} = 1\mathrm{kV.cm}^{-1}$, $E_{\mathrm{I}} = 3\mathrm{kV.cm}^{-1}$, $V_{\mathrm{GEM}} = 400V$ and $r_{\mathrm{P}} = 0.6$ at constant settings.

It can be observed that the gain has an optimal value around the region of $50 - 60$ μm and decreases upon increasing or decreasing the diameter any further. Both the total and effective gains show a similar behavior. The electric field lines leave the top metal with high potential and land on the bottom metal with lower potential. The concentration of field lines is highest when there is no opening or GEM hole and steadily decreases with increasing

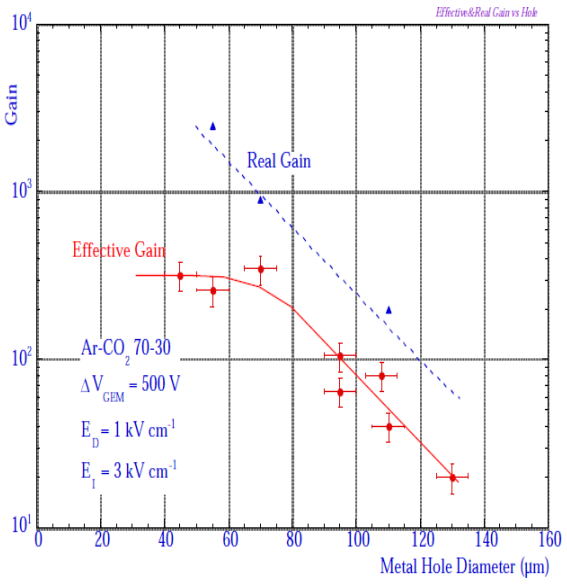

Figure 4.1: Measured gain dependence on GEM hole dia [14].

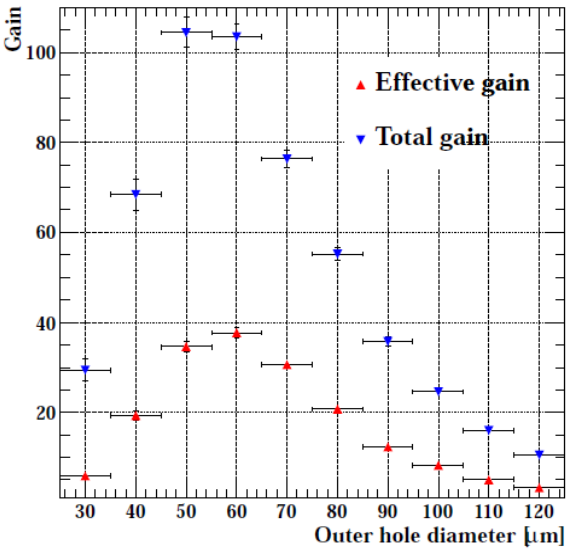

Figure 4.2: Simulated gain dependence on GEM hole dia [1].

hole diameter. Due to this, the amplification and hence gain reduces with increasing hole diameter. This explains the region beyond 60 μm in the plot.

Another factor that affects gain is the optical transparency which decreases with decreasing diameter. With decreasing optical transparency, the likelihood of primary electrons being lost to the top GEM metal increases. This effectively reduces both the total and effective gains. With a smaller hole diameter the space available for electron to freely diffuse is reduced. This enhances losses to the polyimide due to diffusion and reduces the effective gain in the process.

The simulated gain dependence is explained by a trade-off between the aforementioned phenomenon. Lower diameter regions have dominant primary losses and losses to PMD surface while higher diameters suffer from a lowered amplification. Optimal region exists in between the two regions.

The simulation results in this regard are not in complete agreement with measured values from [14], and this can be investigated experimentally by testing newly ordered GEMs with variable diameters.

4.5 Losses of primary and secondary charges

Charge is lost to a GEM through many processes. Losses can be both for primary and secondary charges. The following are the possibly encountered losses-

Top metal Electrons lost to the top metal are usually primary electrons. This is because the avalanche process begins after the primary electrons ventures into the GEM hole and is dominant near the bottom GEM hole towards the exit. As discussed in section 4.4, optical transparency influences the losses to the top metal. In addition, increase in drift field also increases losses.

Bottom metal Losses in the bottom GEM metal are due to the attraction of the generated charges by the metal. These are secondary losses and can be reduced by increasing the induction field.

GEM hole Losses inside the GEM hole occur due to the electrons that diffuse in the gas inside GEM hole causing them to be stuck to the PMD surface. Due to high electron affinity of PMD the electrons cannot diffuse back into the gas medium once stuck to the PMD surface. Losses inside the GEM hole and their effects are discussed in the chapter on charging up.

Attachment Attachment losses occur due to the electro-negativity of CO_2. These losses can occur in all regions where gas is present namely drift gap, GEM hole and induction gap.

4.6 Effect of Drift and Induction field

Effect of drift and induction fields have been simulated by S.Dildick and the results are seen in fig 4.3.

Drift field Drift field is needed to drift the primary electrons generated in the drift gap towards the top GEM metal. The field inside the GEM hole will be responsible for further

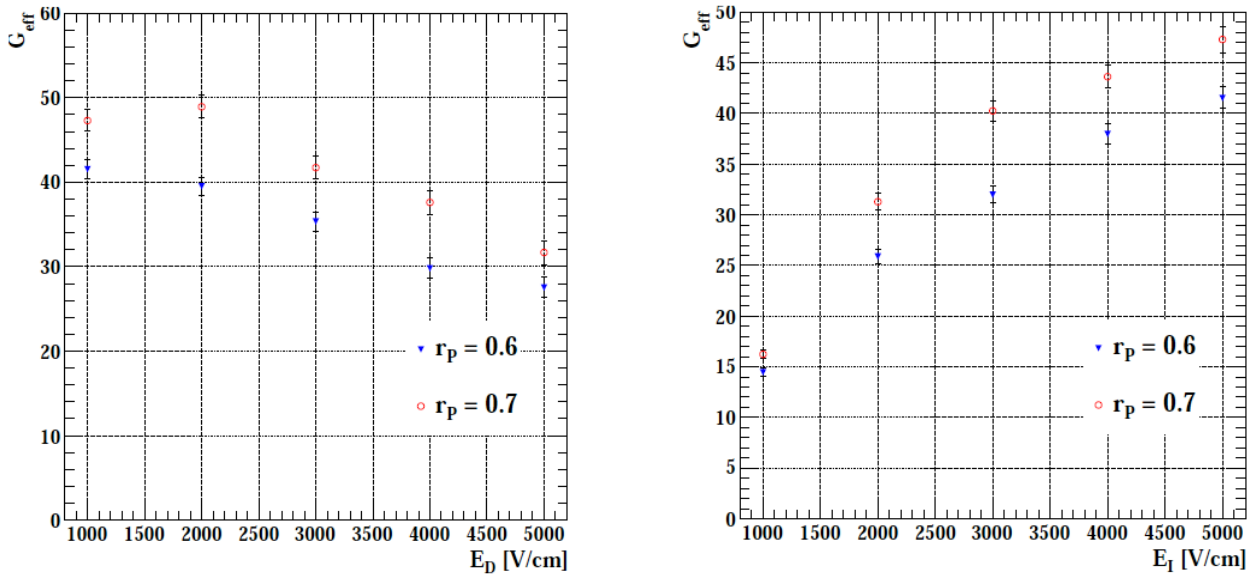

Figure 4.3: Plot of gain as a function of the E_{D} at $E_{\mathrm{I}} = 5$ kV.cm^{-1} (left) and as a function of E_{I} at $E_{\mathrm{D}} = 1$ kV.cm^{-1} (right) for various r_{P} values [23].

attracting the electron into the hole. Hence a strong drift field is desirable to attract the electrons towards the GEM, yet very high fields can cause the field lines to land on the metal instead of inside the hole. This decreases the gain.

Induction field Induction field is set in order to attract the electrons generated in the avalanche towards the readout plane. As the induction field is increased the electrons that would otherwise be lost to the lower metal will be attracted away and this improves the gain.

4.7 Estimation of Penning Parameter

Penning transfer mechanism has been described in the section 3.2. Estimation of penning parameter can be made by comparing an experimentally measured gain curve with simulated gain curves in which penning transfer probability has been left as a free parameter. A gain curve is a plot of gain as a function of the voltage difference across the top and bottom metals of a GEM. This dependence is exponential in nature. Fig 4.7 (left) is an example of an experimentally measured gain curve. Due to the limited availability of experimental data, I performed subsequent measurements for comparison with simulations which enabled

the estimation of penning parameter. These experiments will be described in chapter 6.

Gain curve from experimental data was compared with the simulated gain curves while parameterizing the penning transfer probability (r_{P}). A χ^2 fit was performed for various r_{P} values and the true value was estimated by finding the minima of χ^2. Where χ^2 has been defined as follows-

$$\chi^2 = \Sigma \left(\frac{G_{\mathrm{measured}} - g.G_{\mathrm{calculated}}}{\sigma^2_{\mathrm{measured}} + \sigma^2_{\mathrm{calculated}}} \right)^2 \tag{4.1}$$

Where, G_{measured} is the measured gain, and $G_{\mathrm{calculated}}$ is the calculated gain found through simulation. A gain scaling factor g has been introduced to account for the scaling that often needs to be done when dealing with experimental data. A more complete treatment will include a gain offset factor g_{o} which is added to the calculated gain after scaling with g.

$$\chi^2 = \Sigma \left(\frac{G_{\mathrm{measured}} - g.G_{\mathrm{calculated}} - g_o}{\sigma^2_{\mathrm{measured}} + \sigma^2_{\mathrm{calculated}}} \right)^2 \tag{4.2}$$

Experimental data initially used was obtained from the work of Gabriele [24] presented in his PhD thesis. The gain curve and the χ^2 fit are shown below.

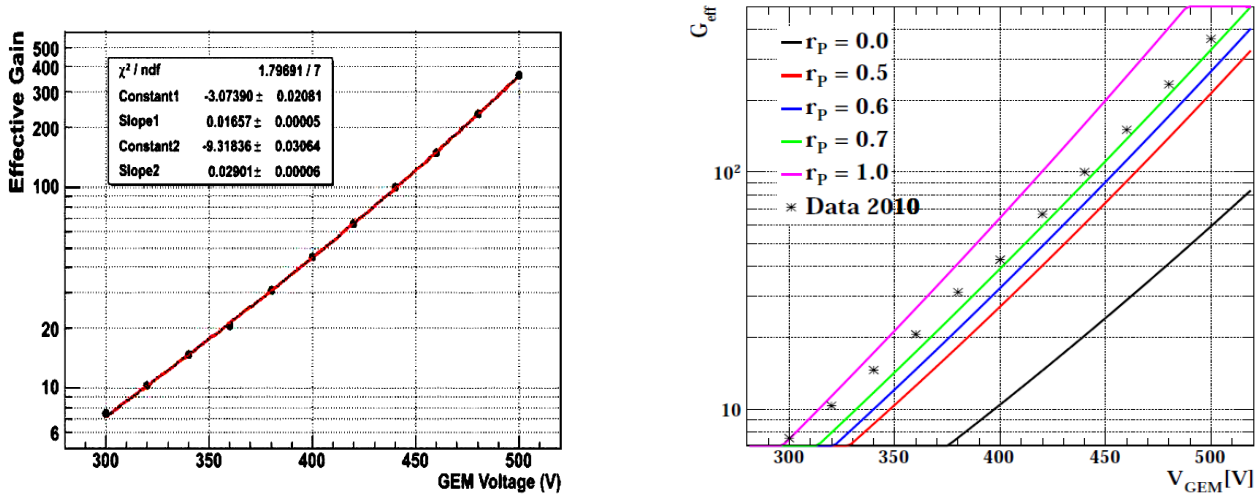

Figure 4.4: Gain curve for $\mathrm{Ar} - \mathrm{CO}_2$ 70/30 mixture measured (left) [24]; and simulated (right) [23]

In the simulated gain curves, the free parameter was the penning parameter and a gain scaling parameter without the introduction of any offset. As a result the simulated gain

curve with $r_P = 0.5$ agrees closely with the data. Although $r_P = 0.7$ appears to be similar, the difference can be observed in the lower voltages where the correlation is non existent. Without the introduction of penning parameter however there is no correlation with the data as can be seen from the black curve for $r_P = 0$. One can also observe that the steepness of the simulated gain curve increases directly with the penning transfer probability.

For accurate estimation of Penning parameter, measurements have been performed for gas mixtures $Ar - CO_2$ 70/30 (Experiment-B) and 90/10 (Experiment-C) that decoupled the charging up effects. The resulting gain curve from those measurements has been termed 'real gain' due to the appropriateness of its comparison with simulated gain. Through the χ^2 fit one can observe the degree of correlation the simulated data has with the measured data. The χ^2 fit showing a minima as the optimum penning parameter can be seen in fig 4.5 and fig 4.6. The gain scaling parameter which is a ratio of experimental gain and the calculated gain has been estimated and plotted alongside the χ^2 fits. The scaling parameter has an expected linear behavior. The values computed are also in agreement with the recent findings in literature. Note that $r_P = 0.7$ is higher than the previous estimate ($r_P = 0.5$) for the 70/30 mixture. Table 4.2 lists the estimated values of Penning parameter.

Gas mixture	r_P
$Ar - CO_2 - 70/30$	0.70
$Ar - CO_2 - 90/10$	0.45

Table 4.2: Estimated values of Penning transfer parameter r_P for $Ar - CO_2$ mixtures.

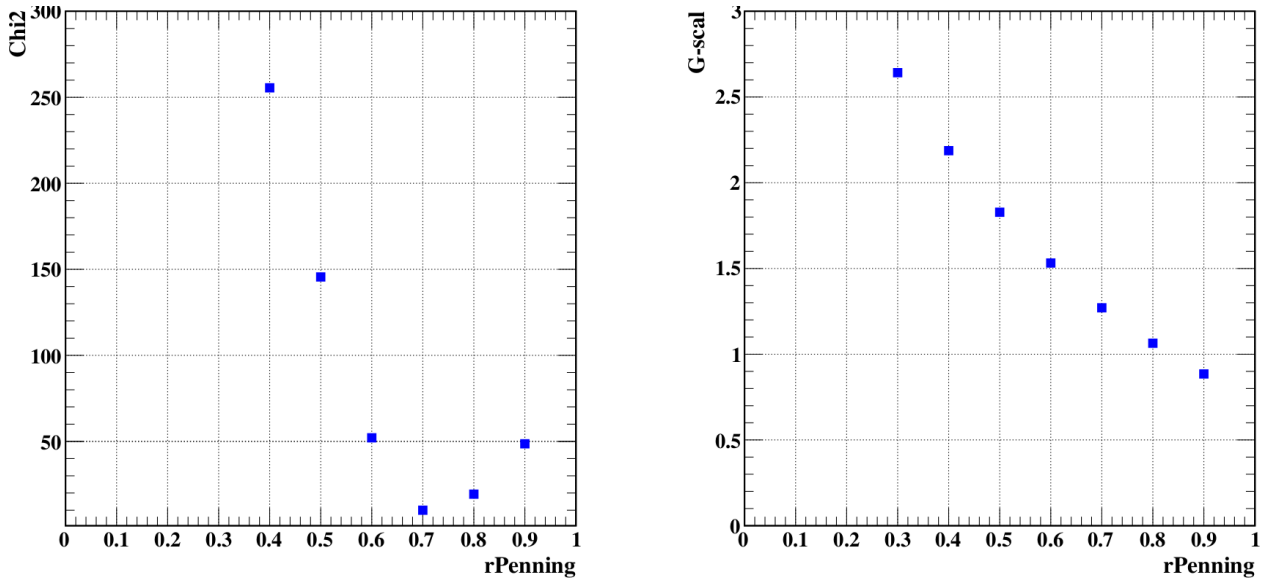

Figure 4.5: Left: χ^2 as a function of r_{P} for $\mathrm{Ar}-\mathrm{CO}_2$ 70/30 mixture, Right: Gain scaling parameter as a function of r_{P}

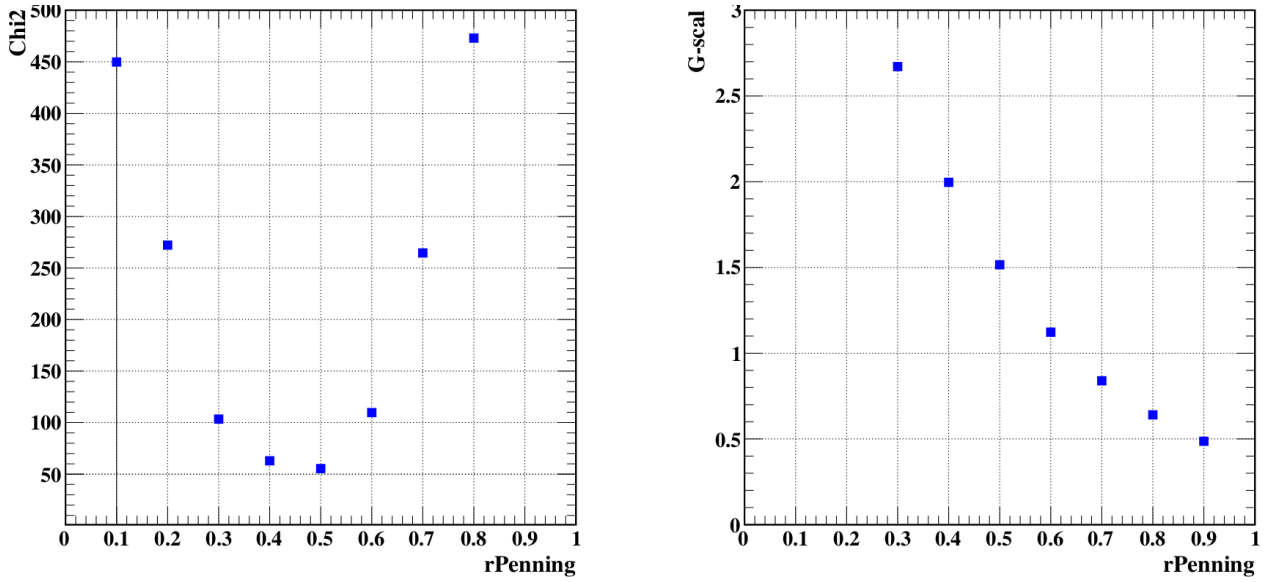

Figure 4.6: Left: χ^2 as a function of r_{P} for $\mathrm{Ar}-\mathrm{CO}_2$ 90/10 mixture, Right: Gain scaling parameter as a function of r_{P}

5 EXPERIMENTAL TECHNIQUE AND GAIN CALIBRATION

Experimental setup, methods and techniques employed for this research work including the gain measurement and calibration procedures have been discussed in this section. The normalization procedures employed in the lab, and those that were specifically conceived for the charging-up measurements are separately described.

5.1 Setup

In order to measure the GEM gain there are two phases involved - calibration and measurement. Calibration is a voltage measurement through which the normalization factor is obtained. The normalization factor is then multiplied with a measured current to obtain gain. Some aspects of the setup are common to both stages of measurement.

GEM is mounted on a 'Timing GEM chamber' as shown in the fig 5.1. The chamber has

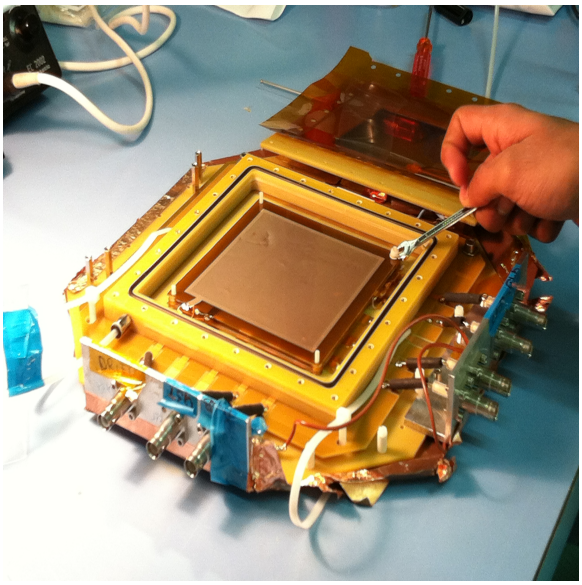

Figure 5.1: GEM foil being mounted on a timing GEM chamber

inlet and outlet for the circulation of gas mixture. The ratio of each gas in the mixture is controlled through a potentiometer based system. Gas flow rate is set to 6 l/hr. The pressure inside the chamber is maintained at 760 Torr. The chamber has a kapton window to allow the incidence of Xrays and to be able to withstand pressure differences with respect to external

conditions. X-ray photons of 8 keV are incident as ionizing radiation from the PANalytical Xray machine as shown in Fig 5.2 (left). The readout strips located below the GEM plane are shorted and maintained at ground potential. High voltage is applied across the GEM top and bottom electrodes and to the drift plane. Fig 5.3 depicts the experimental setup for both the measurement phases.

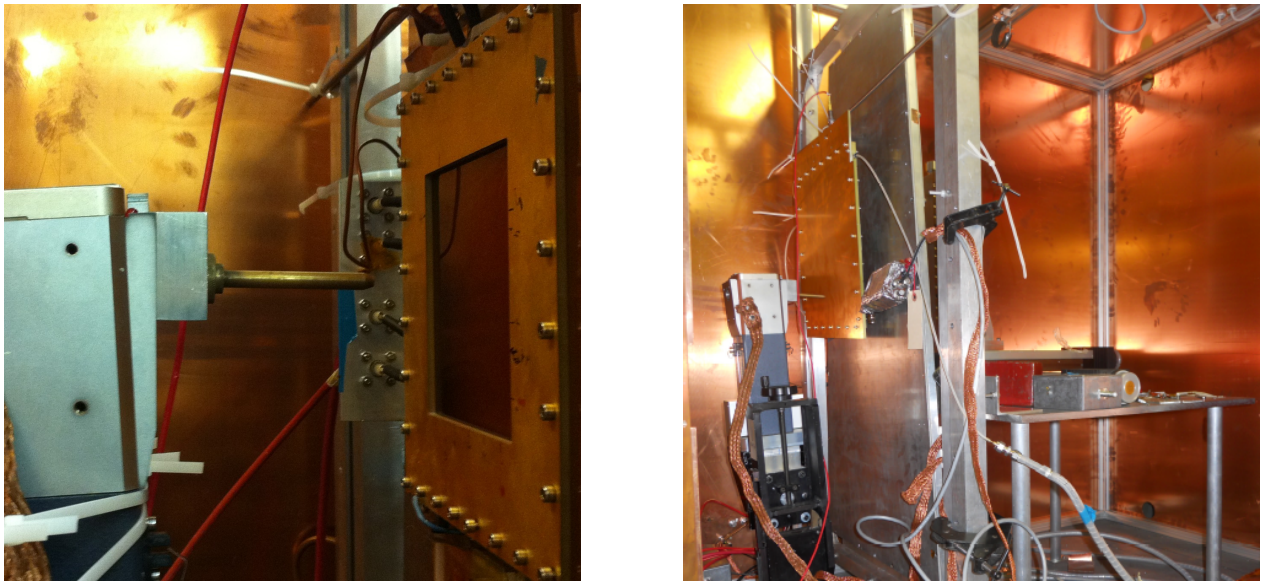

Figure 5.2: Left: Collimator positioned normal to the GEM surface. Right: GEM mounted inside a Faraday cage [25].

Parameter	**Gain calibration**	**Gain measurement**
Voltage (V)	520	$200 - 520$
I_{Xray} (mA)	0.6	1.6
V_{Xray} (kV)	10	10
Collimator dia (mm)	2	1
Absorber	Cu (68 μm)	-
Temperature (K)	300	-
Absorber	Cu(68 μm)	-

Table 5.1: Settings used in gain calibration and measurement

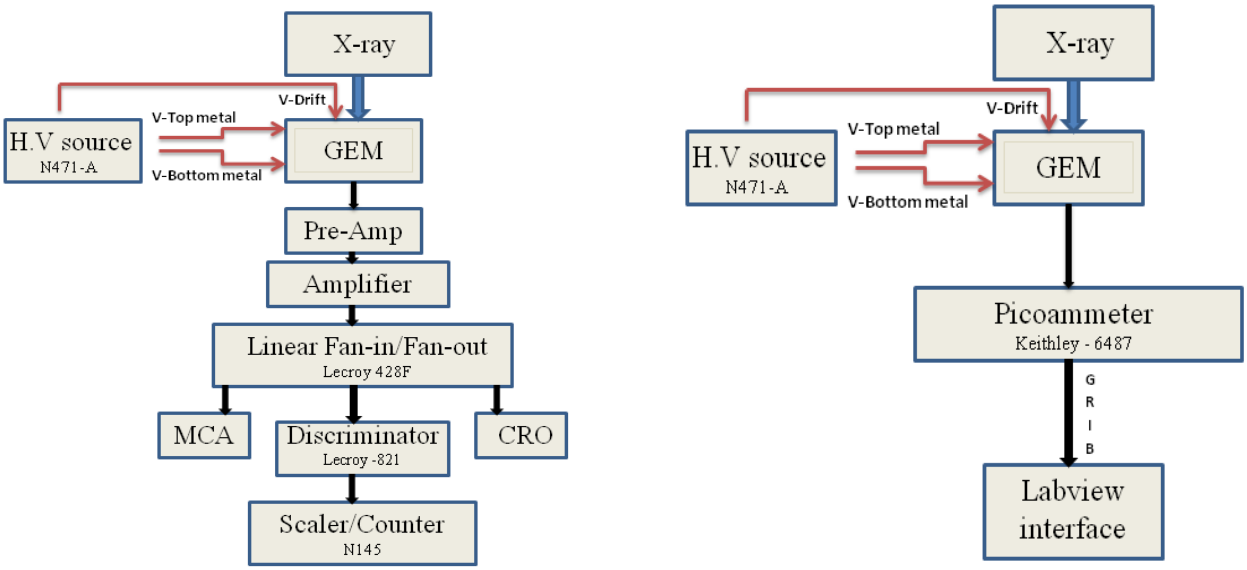

Figure 5.3: Flow chart depicting the setup for Gain calibration (left) and Gain measurement (right)

5.1.1 Gain calibration

In order to make a voltage measurement of the signal, a resistance of 1 MΩ is connected across the readout and the ground. Since the signal across this resistor is weak, a pre-amplification stage is set initially. The signal then is carried to the amplifier ORTEC 450 for a second stage amplification. Amplifier output is then fed to the linear fan-in/fan-out Lecroy-428F which generates multiple copies of the signal to be analyzed through various channels as seen in fig 5.3 (left). Through a Multi Channel Analyzer - Amptek 8000A, the pulse height spectrum of the signal is obtained and recorded on a computer through an interfacing software ADMCA (available for download from Amptek software downloads page [26]). Signal can be visualized through a CRO. Signal is also fed into a discriminator Lecroy-821, with a set threshold value. The discriminator output is a digital pulse which is a high for the signals crossing the threshold and a low for the rest. By feeding this output to a scaler N145, a count of the number of signals in a given time (usually set to 30s) is recorded.

The MCA and the scaler are subject to a condition called pile-up. Pile-up refers to the overlap of consecutive signals which are not treated as different by the electronics since

the time difference between consecutive signals is comparable to the response time of the electronics. Presence of pile-up can distort the MCA spectrum or cause a smaller number of signal counts to be measured.

Method GEM is left under the circulation of gas mixture for one hour. During the same period it is also kept under 500 V on a high voltage supply. This voltage is chosen to be lower for higher percentages of Ar to avoid discharges. Xray machine is turned on and the standard settings of current and voltage for a calibration are set while the shutter is still kept closed. When the Xray photons are incident on the GEM it gives rise to a voltage signal that can be observed on a CRO. If the signal is not visible or appears noisy, proper grounding is ensured to eliminate the noise. A pulse height spectrum is then obtained by using the MCA. A clean signal has a prominent photo-peak, a clear escape peak, a noise pedestal each of which are well separated from one another. Poor spectra are a result of pile up which occurs due to excessive input signal, contrarily they can also signify a complete lack of signal.

Starting from around 360 V, the counts of number of pulses of signal are recorded using the scaler over a period of 30 s. The measurement is repeated thrice for better accuracy of the estimate. Counts are recorded for various settings through increments of voltage. Since a finite number of photons are incident on the GEM, the same number of pulses are obtained at the output. For lower voltages across the GEM, the amplification or gain is lower. This is coupled with large losses, as a result all the incident photons do not translate to the counts of the pulses measured. A plateau of the voltage counts is obtained after a sufficient voltage is applied across the GEM. Increasing voltages beyond the plateau region will result in sparks due to discharges and hence are avoided.

A voltage is chosen in the region of operation for the calibration measurement. Counts are obtained with and without absorber for a low current 0.6 mA on Xray, and with absorber for a high current 1.6 mA. Through these measurements, the counts at high current are obtained without absorber. This will determine the normalization factor for the current measurement which is performed on a high Xray current without absorber. The absorber used in these

measurements is usually a copper tape with 68 μm thickness. Two layers of the tape are used for the setting with absorber. [1]

5.1.2 Gain measurement

A current measurement is performed by measuring the current at the anode of a GEM directly without any intermediate amplification. The schematic is shown in fig 5.3 (right). Keithley -6517 measured the anode current and the values are fed into computer through a GRIB interface. A lab-view interface (developed by Matteo Alfonsi) reads and records the current values from the GRIB. Through the lab-view interface the sampling rate of the current can be adjusted. The values of current versus time are recorded on a text file which is later analyzed through root scripts.

An important difference in current measurement lies in the rate of incidence of Xray photons. Due to extremely low currents and the lack of amplification at the output stage, it is essential to increase the strength of input signal in order to have a higher current. In addition there is no risk of a pileup as the measurement pertains only to the total charge collected at the anode. This increased incident flux is achieved by one of the following methods:

- Increasing the current on Xray
- Using a bigger collimator

Method Once the connections have been made according to the flowchart shown in fig 5.3 (right), the Xray is incident on the GEM and the current is recorded on a text file with a sampling time of 2s. An arbitrary voltage well below the plateau is chosen as a starting value for the measurement. Currents are then recorded for voltages increasing in steps of 20V upto the region of discharge. Typical range of voltages for measurements are $300\text{V} - 520\text{V}$. From

[1] The above mentioned method is the standard calibration technique practiced in the research group. Changes have been implemented for specific measurements in order to compute the normalization, these will be discussed in later sections.

these measurements one obtains the current vs voltage data which when normalized yields the gain curve.

5.2 Xray machine

The theory of Xray generation has been discussed in section 3.3. The pulse height spectrum obtained for the standard gas mixture was analyzed in detail by performing fits for the lines as shown in fig 5.4. Since a $Cu - K_\alpha$ Xray photon is the ionizing particle being detected,

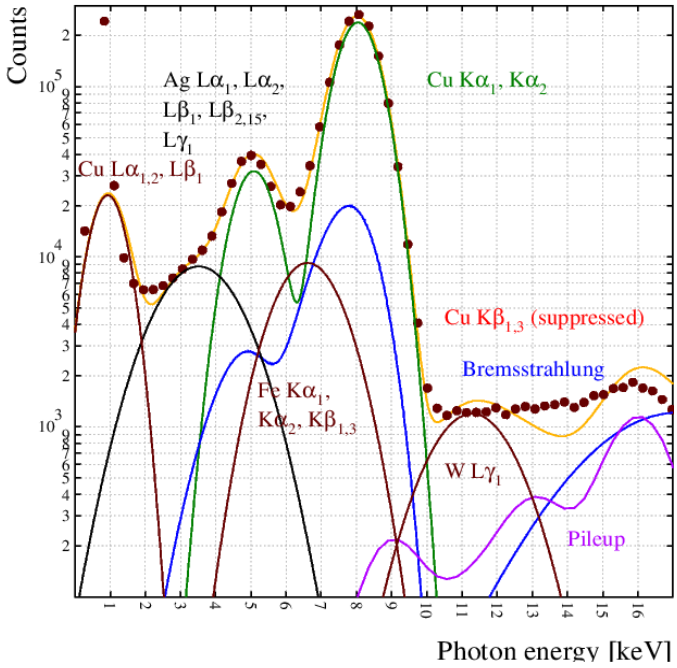

Figure 5.4: Fit to MCA spectrum revealing the presence of lines corresponding to various elements. Relative line normalizations and energies were set from the X-ray booklet [27] and Bremsstrahlung was obtained from G.Castellano [28].

there are standard lines that are expected. These include the photo peak, the escape peak, Bremsstrahlung radiation and the pile up resulting from signals spaced closely in time. However, the fit performed revealed the presence of other lines in the spectra which were usually not expected. A detailed analysis of the Xray tube's constituents and a correspondence with the Xray manufacturer 'PANalytical' provided insights into the functioning of the Xray tube. The schematic diagram shown in fig 3.2 will serve as a reference to the understanding. Cath-

ode tungsten filament when heated emits electrons. These electrons in turn hit the copper anode to give rise to Xray photons. Increasing the current on X-ray cathode increases the photon intensity proportionately due to greater number of incident electrons on the copper target. It has been warned by the manufacturing company that a consistent usage of high current on X-ray can be a means of depositing sufficiently large amounts of tungsten (used to make the cathode filament) on the inner walls of the X-ray tube including the anode [29]. Since the process of Xray generation is extremely inefficient, most of the electrons deposit the energy to the copper anode causing it to heat up. Since the copper is placed on a Ag substrate, the intense heat causes the silver to diffuse into the copper bringing it to the forefront. This occurs in spite of ample cooling provided by water running constantly in the background of the substrate. Presence of silver in the anode produces Xray photons corresponding to silver.

The tube structure in addition also contains Iron which gives rise to Fe lines in the spectrum. All the additional components give rise to their respective spectral lines in varied quantities in addition to the K_α as can be seen in the fit to MCA.

The dependence of X-ray output intensity on Current has been measured in order to calibrate the machine for various settings that have been used for different sets of measurements. These can be observed in the fig 5.5 (left).

5.3 Normalization: Laboratory technique

Gain is an estimate of the number of charges reaching the anode of a GEM per incident primary electron. The measured quantities are the output current, the spectra from Multi Channel Analyzer (MCA) and the counts of Xray photons.

For basic estimation of normalization factor, the MCA spectrum is not considered. Input charge can be estimated from the counts of Xray for high current on Xray computed according to the method described in section 5.1.1. The number of primary electrons (N_{primary}) created per incident photon depends on the photon energy and the work function of the given gas

mixture.

$$N_{primary} = E_\gamma \times \left(\frac{\%Ar}{W_{Ar}} + \frac{\%CO_2}{W_{CO_2}} \right) \tag{5.1}$$

Where $E_\gamma = 8.03$ keV is the energy of the incident Xray photons, %Ar and $\%CO_2$ are the percentages of the gases in the mixture, W_{Ar} and W_{CO_2} are the work functions of the gases. Estimation of gain includes output current, number of primaries and the electron charge.

5.4 Normalization: Charging-up measurements

There are two settings for which the current measurements have been performed for charging-up measurements as a part of 'experiment – C' described in section 6.3. Table 5.2 summarizes them in comparison with the calibration settings. The MCA counts enable the calibration

Parameter	**Calibration – C**	**Measurement – C.1**	**Measurement – C.2**
Voltage (V)	520	200 – 300	300 – 460
I_{Xray} (mA)	0.6	9	4
V_{Xray} (kV)	20	20	20
Collimator dia (mm)	2	8.8	8.8
Absorber	Ni	Ni	Ni

Table 5.2: Comparison of measurement and calibration settings for experiment – C performed with a low photon rate per GEM hole.

of gain through normalization. This procedure involves various steps.

X-ray scaling In order to avoid pile-up while measuring the MCA spectra, a lower photon rate is chosen when compared to the current measurement. Normalization also comprises the estimation of counts for the settings of current measurement by scaling. To obtain this scaling factor, X-ray counts have been measured for various settings of I_{Xray} and the rates are plotted as shown in the fig 5.5(left). The photon counts are measured by the scaler N-145. For high currents(4 mA and 9 mA) used on X-ray, the counts are not in the linear region of operation presumably because of a pile up. This outcome was in spite of using a sufficient absorber

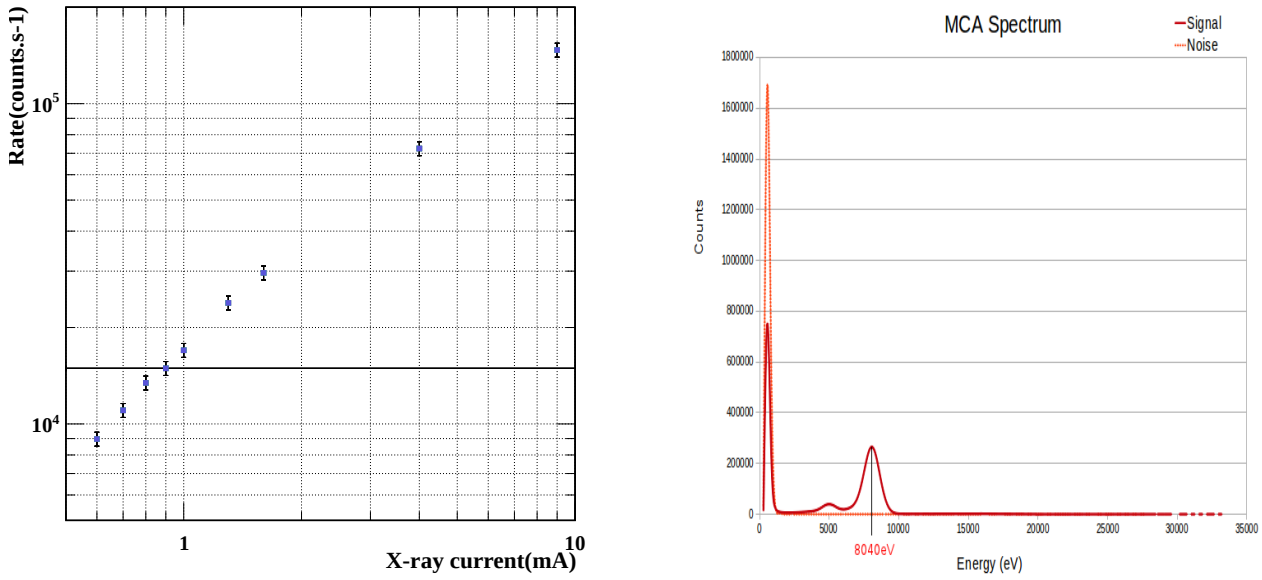

Figure 5.5: Left: Dependence of photon rate on the applied cathode current of the X-ray tube. Right: Comparison of spectra with(red) and without(orange) X-ray irradiation

material to avoid pile up. Counts for lower currents on X-ray however show a linearity. Extrapolation of the linear region is used as a basis for estimating the correct photon rate for the high currents on X-ray. The factors 19.41 and 8.45 are respectively obtained for the number of times the counts for settings A and B are higher than the MCA setting at a given collimator size. In addition, a smaller collimator of 2 mm diameter has been used for MCA measurement as against 8.8 mm dia for current measurement. This introduces a multiplicative factor equal to the ratio of areas of the two collimators since the photon flux is proportional to the area.

Noise The counts from the MCA spectrum include both signal and noise while the latter is predominant in the initial channels. In order to isolate noise from the signal, spectra is taken without incident X-ray. A comparison of both counts is seen in the fig 5.5(right). It can be inferred that the noise counts(pertinent to the lower bins) are smaller with the application of X-ray. This can be explained by a possible loss of counts due to the overlap of noise with the signal counts. Noise counts in the signal have been observed to be a factor 0.41 times lower than in the pure noise spectrum in the three major channels. Noise was scaled by this

value and subtracted from the signal. In addition, a lower channel with energy 551 eV that contributed to some counts was suppressed.

MCA The number of primary electrons created per incident photon is estimated by analyzing the MCA spectrum. By fitting the photo and escape peaks, energies of individual channels are calibrated. Number of electrons contributed by individual channel is obtained from equation 5.2.

$$\sum_i \left(\frac{N_i}{\Sigma N_i} \times \frac{E_i}{W} \right) \sim 280 \tag{5.2}$$

Where N_i is the number of counts and E_i is the energy corresponding to i^{th} channel of MCA. W is the work function of $Ar/CO_2 - 70/30\%$ mixture as obtained from fig 5.6. A weighted sum of the number of electrons from each channel is computed to obtain a value of 280 electrons per photon.

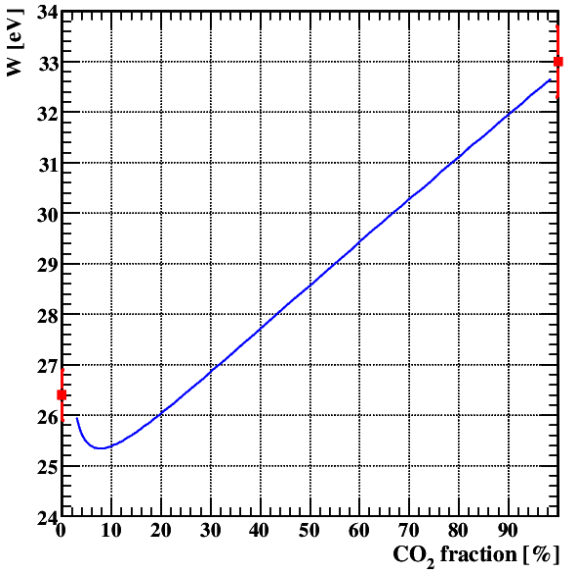

Figure 5.6: Penning corrected work function for $Ar - CO_2$ mixtures computed by Heinrich Schindler using Magboltz[12]

.

The total number of counts measured in the MCA spectrum after noise subtraction is 1.7 MHz over a period of 78 s. This number forms a basis for the estimation of counts at the gain measurement settings.

Dark current Laboratory measurements are performed using X-ray source, photons entering the drift gap cause primary ionizations. These electrons under the influence of drift field enter the GEM holes undergoing avalanche multiplication before being read out at the anode. There however exists a finite probability that the photons interact with the gas in the induction gap causing further ionizations. These ionizations cause a dark current which persists even during the complete absence of amplification. Taking into account the attenuation coefficients and densities of the materials, the optical transparency and the dimensions of the GEM including the drift and induction gaps, dark current is estimated. X-ray scaling which was performed at 520 V has counts dominated due to interactions in drift. Using the previous ratio, the interactions in the induction gap can be estimated for both settings at which current measurements have been performed. Comparison of scaling and dark currents can be seen in table 5.3

Parameter	**Measurement – C.1**	**Measurement – C.2**
X-ray scaling factor	19.41	8.45
Dark current(nA)	-0.17	-0.07

Table 5.3: Comparison of scaling parameters and dark currents for the two measurement settings used in experiment – C

5.5 Gain stability

Measurements are performed in order to test the long term gain stability of the detectors. Using a high current(1.6 mA) on Xray and an applied voltage chosen from the plateau region, gain is recorded continuously for a period of 1 hr. Another method implemented in this regard is the measurement of rate capability. This is done by recording continuously the pulse height spectra at specific intervals over a large period of time . The photo peaks are subsequently computed for each spectrum and are arranged in time. This reveals the change of gain over time since the photo-peak channel is a depiction of the detector gain.

6 CHARGING-UP STUDIES

It has been observed in previous studies that the gain of a GEM varies over time in spite of uniformly maintained ambient and applied conditions. This variation has been attributed to either the charge deposition inside GEM holes or the polarization of ions constituting the polymer PMD [30]. Both aspects have been dealt with in this study.

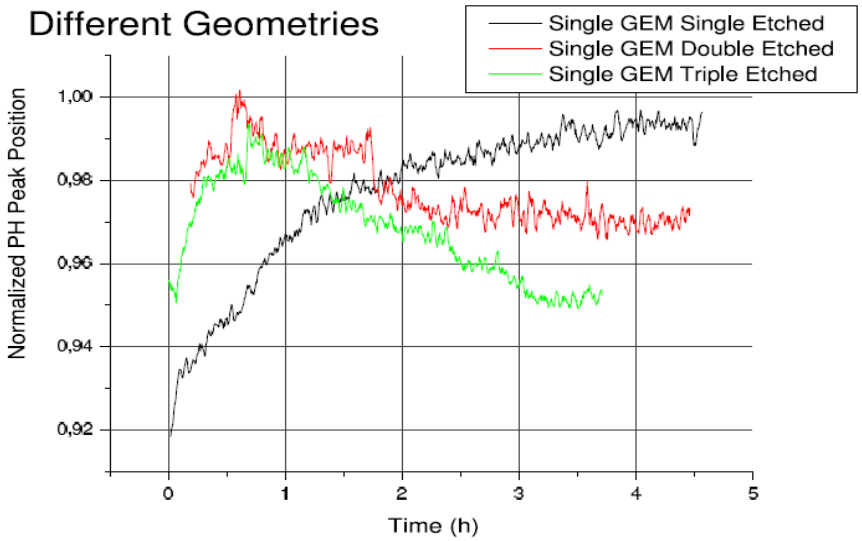

Figure 6.1: Gain variation seen as due to charging up [30]

The exact physics behind this was poorly understood and varied reports of the same are found in literature. Tamagawa et al. [31], claim that cylindrical geometry of the GEM hole results in a stable gain behavior over time. A biconical hole structure such as in standard CERN single GEMs on the other hand results in a rapid increase followed by a relatively stable gain as observed by J.Benlloch et al., [32]. In most of the reports, an initial increase in gain was followed by a stable phase.

Studies in this chapter were performed with the aim of systematically analyzing these effects which are termed as charging-up effects. A model was also developed for the same. Three sets of experiments (listed below) were performed and each result led to an improvisation of technique for the successive measurement. Experiment – A was done in collaboration with Laura Franconi and Dr.Renju Thomas. Experiment – B was done in collaboration with

Özkan Şahin and Yalçın Kalkan.

- Experiment – A (Oct 2011)
- Experiment – B (Nov 2011)
- Experiment – C (Dec 2011)

6.1 Experiment – A

During the October-2011, measurements of gain for various gas mixtures were performed. This included $Ar - CO_2$: 70/30; 50/50; 80/20; 90/10. The original aim was to compare the measured gain curves for different gas mixtures with the simulated gains to compute the penning parameter for these mixtures. Observations of certain effects led to the conduction of a systematic study to understand charging up in GEMs.

6.1.1 Setup

Experimental set-up used for this measurement is the standard one described in section 5.1

Method For every gas mixture chosen, gain calibration was performed as described in section 5.1. After the GEM was mounted and kept under the voltage supply, X rays were irradiated on the same spatial region of the GEM for all measurement voltages for a given gas mixture. A starting voltage for measurement was qualitatively chosen around 100 V below the plateau region of count. During the October-2011, measurements of gain the various gas mixtures were performed. This included $Ar - CO_2$: 70/30; 50/50; 80/20; 90/10.

6.1.2 Observation

Fig. 6.2 shows the gain curves for the measured current pertaining to the gas mixtures chosen. All curves exhibit a behavior of scaling or offset of the gain values for voltages above and

below the starting voltage of measurement. This can be markedly observed in 90/10 mixture where the V_{start} was 300 V.

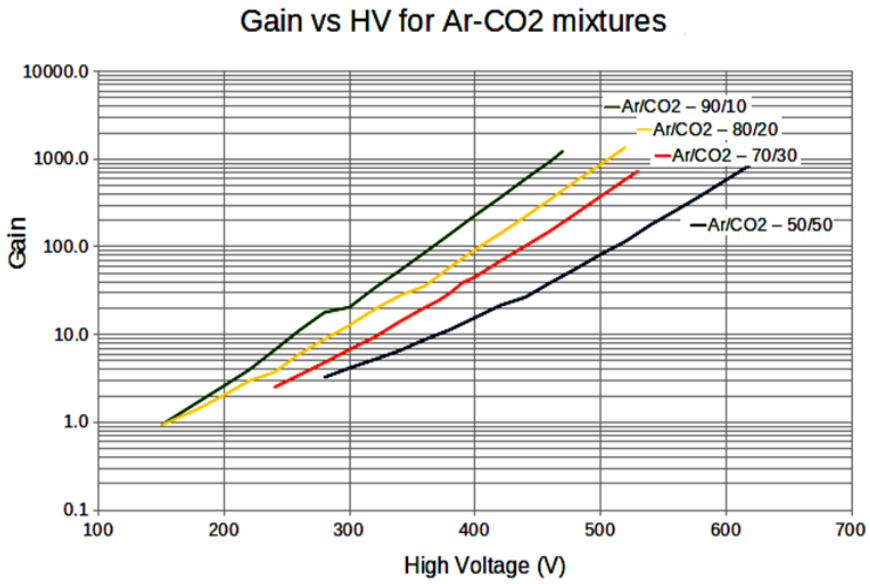

Figure 6.2: Gain curves for various gas mixtures

The current measured by the Keithley-6257 showed oscillations with a period of ~ 19 as seen in the fig. 6.3. A Fourier analysis was performed on the current to verify the oscillation frequency. A spike can be observed in the Fourier spectrum at ~ 0.05 Hz which was due to oscillations.

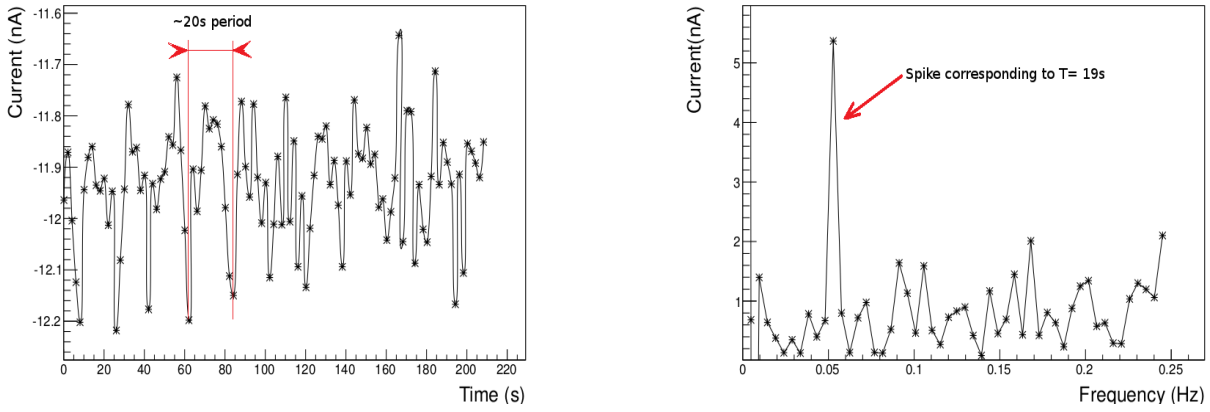

Figure 6.3: Left: Oscillations exhibited by the current, Right: Fourier transform of the measured current

The current showed a decrease of $15 - 30\%$ for lower gains. For higher gains increases

upto 5% were found although majority remained fairly uniform for the higher gains as seen in fig. 6.4. Observation of measured currents for individual voltages showed that current decreased over time for voltages below V_{start} while currents increased slightly or remained constant for values higher than V_{start}.

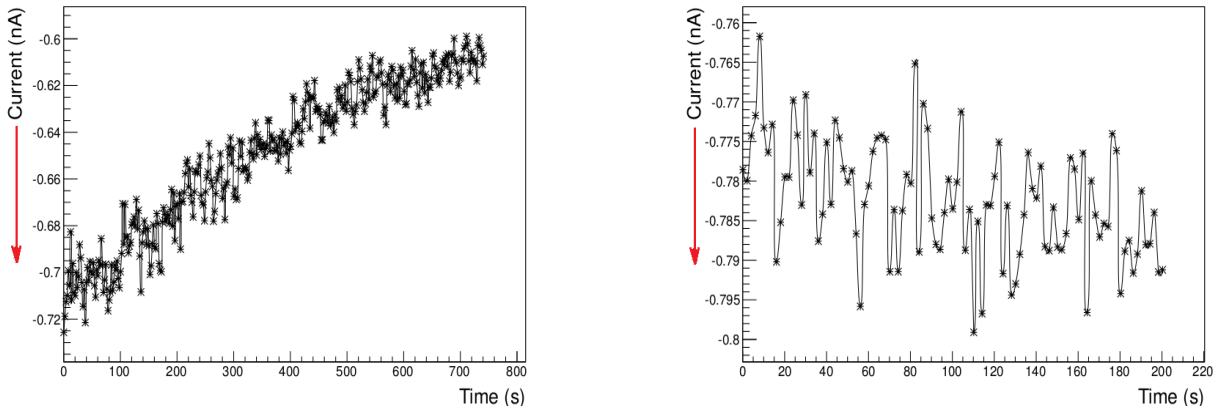

Figure 6.4: Current vs time for $Ar - CO_2$ 80/20 mixture measured at 340 V(left) and 360 V(right)

6.1.3 Analysis

Electronic noise and Keithley pico-ammeter settings were likely candidates for the cause of oscillations in the current. Electronic noise is not usually in the sub-hertz range. Keithley device manual did not provide any reference on possible oscillations. The source remains unknown although similar measurements performed later did not give rise to these oscillations.

Marked change in the trend of the measured current can be attributed to the choice of V_{start} as the initial measurement setting. In addition, the same spatial point on the GEM foil was being irradiated for all voltage settings. Due to this a cumulative effect of the previous measurements would be observed on a given measurement. A possible hypothesis was that the GEM was charged-up in the process of measuring higher gains and the fields are significantly altered for subsequent measurements for voltage settings below V_{start}. The process of charging up will be explained in detail in the section 6.2.2.

Due to the effects observed, the data obtained was rendered unfit for further analysis and hence another set of measurements were performed as described in the next section.

6.2 Experiment – B

In the November-2011, gain measurements were performed for gas mixtures $Ar - CO_2 : 70/30$ and $90/10$.

Method In order to decouple the effects of various settings, gain measurements at every voltage were performed on a separately irradiated spatial point on the GEM foil. This was achieved by changing the position of the X ray collimator along the plane parallel to the GEM foil. For each setting, voltages and electric fields are applied across the GEM and left for 5 minutes before Xrays are irradiated. Current is continuously and monitored through the labview interface. The amplified signal present only during the presence of Xray is recorded for a period of 30 minutes for each setting to have sufficient time to observe the changes in the gain due to charging up. Table 6.1 describes the settings used in the measurement.

Parameter	**Value**
Collimator dia(mm)	1
Xray current(mA)	1.6
Xray voltage(kV)	10

Table 6.1: Settings for the current measurement to estimate gain (experiment – B)

6.2.1 Observation

The measured current exhibited a certain trend. For lower voltages, the anode current initially increased over time and reached a maximum. This was then followed by a much slower drop in the current. As the voltages were increased to higher values, the rise occurred faster. Beyond a certain applied voltage only drop in the measured current was observed while no increase was seen. This has been interpreted as a possibly sharp rise that occurred

within the current sampling time effectively rendering it unobservable. After sufficiently long time the signal did not show any signs of stability although much less steeper.

6.2.2 Charge-up model

A model was constructed in order to understand the reasons behind the observed rise and drop in the gain, and the dependence on the voltage applied and the irradiation. To construct such a model it is essential to understand the behavior of losses.

The electrons passing through a GEM hole and getting amplified act under the influence of drift and diffusion. Drift occurs due to the applied electric field, while the diffusion occurs independent of the presence of any field. Diffusion of the charges in the gas medium is responsible for the losses inside the GEM hole. Through simulations one can get a picture of the pattern of these losses and their voltage dependence. When charge gets deposited on the PMD surface inside the hole, it does not move along the surface even under the influence of voltage and tends to stay owing to the high resistivity of the GEM. It also does not get diffused back into the gas owing to the high electron affinity of PMD. Details of the conductivity process will be discussed in detail in section. 6.4. Presence of sufficient number of charges causes a noticeable effect on the net electric field inside the GEM hole. Depending on the location and amount of charge accumulated it can either cause an increase or decrease in the amplification.

Losses A portion of the generated electrons are lost to the PMD and this can be estimated from simulations. Fig. 6.5 gives an estimate of the percentage of the effectively generated electrons that are lost on PMD as a function of voltage. It can be observed that the fraction is lower for higher gains and this can also be noticed in the effect it has on gain.
In order to get an estimate of the rate of charging up a typically measured current for a setting can be chosen. For $Ar - CO_2 - 70/30$ mixture, anode current of 2 nA was measured at 460 V. A collimator of 1 mm diameter was used to irradiate Xrays. This corresponds to a

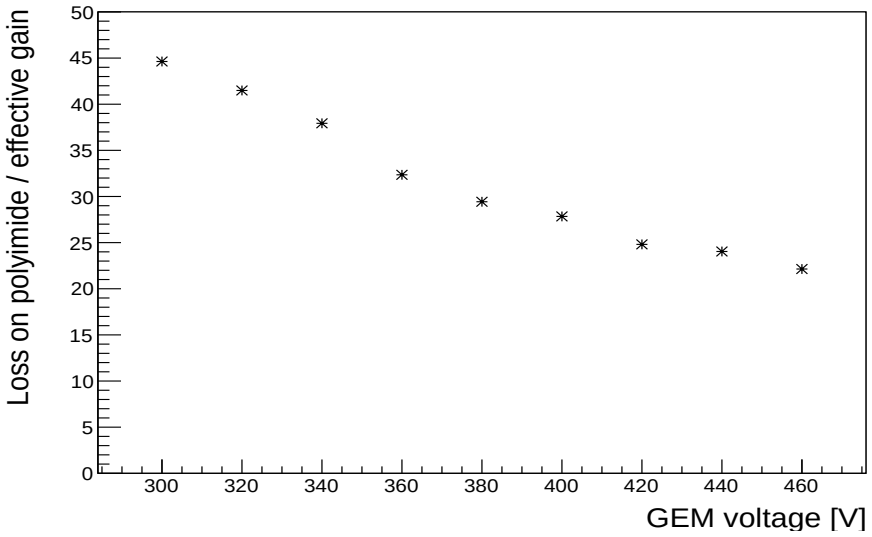

Figure 6.5: Percentage of effectively generated electrons lost to PMD as a function of applied voltage for $Ar - CO_2 - 70/30$ mixture

circular area encompassing ~ 45 GEM holes that are irradiated. At this rate, each GEM hole is accruing charge at the rate of $\sim 6 \times 10^7$ e^- per second. If this rate continues uniformly, the GEM holes will soon have sufficient charge to render amplification impossible. Hence the rate of losses must decrease over time.

Low gain For measurements with low gains one observes an increase in the gain followed by a decrease. This can be explained by analyzing the loss deposition patter as shown in fig 6.6.

Majority of the deposition occurs at the waist of the GEM hole or the region mid-way between the entrance and exit holes. Accumulation of these charges distorts the field causing a lensing effect that focuses the charges. In addition it also aids in reduction of losses to PMD that occur due to diffusion. This results from the repulsion electrons face while approaching the inner hole. As a result of these effects, the GEM gain increases. This accounts for the observed increases seen in the low gain regions.

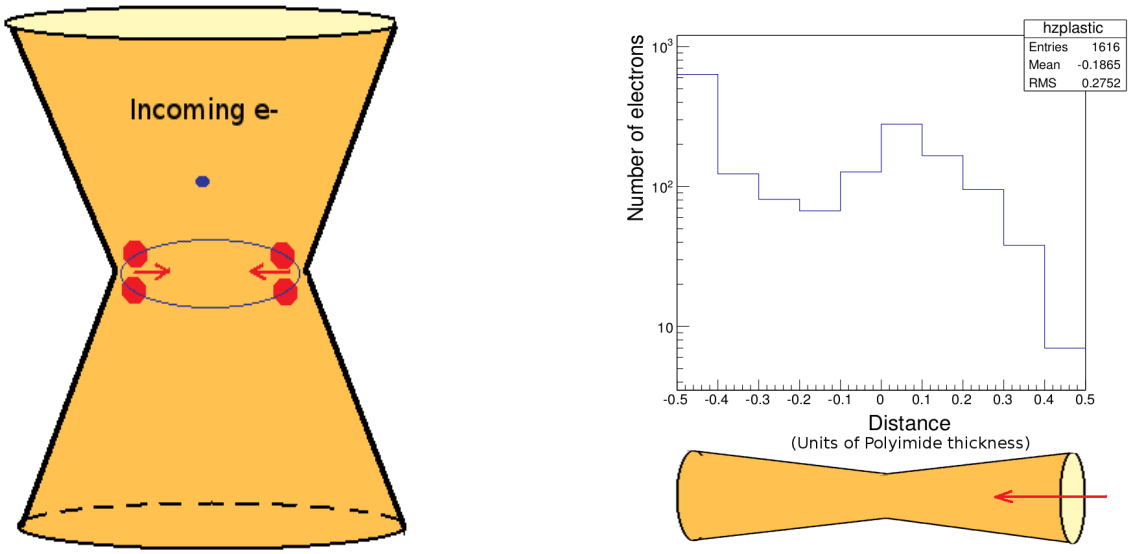

Figure 6.6: Left: E-field due to e^-s on PMD opposing the incoming electron loss at 300 V; Right: Histogram of loss distribution on PMD along the axis at 300 V.

High gain In the high gain regions, a sharp decrease in current is observed. In addition, currents measured in a low gain region decrease after the initial increase reaches a maxima. These observations can be accounted for by analyzing the loss distribution over PMD for higher gains as shown in fig 6.7

Loss pattern distribution reveals that the bulk of charge deposition occurs near the bottom GEM hole. Amount of charge at the bottom GEM hole is around 20 times higher than the charge near the waist. This causes an effective electric field that opposes the electric field responsible for amplification and gain. The avalanche generation is most likely to occur close to the bottom GEM hole where the presence of metal rims cause sharp electric fields. Charge deposition in the lower half of the GEM hole will push the charges away from the surface effectively reducing the possibility of electrons to get closer to the bottom hole and thereby generating avalanches. The entire process effectively results in a reduction of gain that can be observed for higher gains.

Absence of gain increase in higher voltages For higher voltages, the charge deposition occurs rapidly due to a high gain. In this process the first region of gain increase is extremely

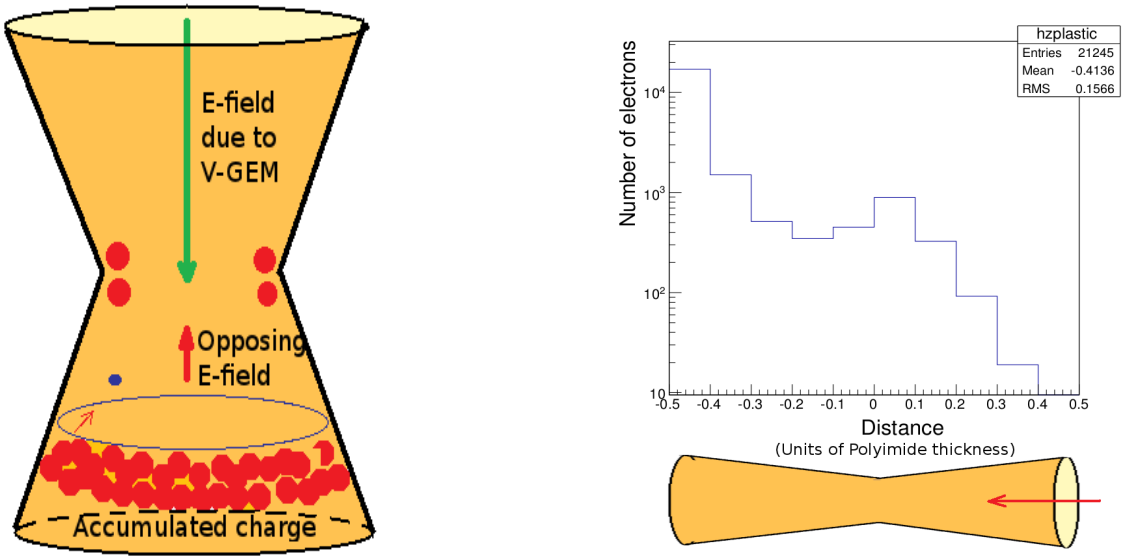

Figure 6.7: Left: Large accumulation of e^-s on PMD at 460 V causing an opposing electric field; Right: Histogram of loss distribution on PMD along the axis at 460 V.

short lived and hence the second region (gain decrease) quickly takes over within the current sampling time of the measuring device. This renders the region of increase unobservable at the measured rate of charging up.

6.3 Experiment – C

In order to verify the functionality of the model presented above, it was essential to measure an initial increase in the gain even at higher voltages. To achieve this the charging up process had to be slowed down either by observing the current in finer time steps or by reducing the incident photon rate. Both the techniques were implemented and measurements were performed.

Reduction of incident rate reduces the number of charges accumulating in a single GEM hole over time and hence the pattern of charge-up making it possible to observe the initial rise in the current. But this proportionately reduces the measured current taking it from nano range to pico range. Currents of this order compete immensely with noise and do not provide reliable information. To circumvent this problem a bigger collimator for Xray was

used while keeping the incident rate low.

6.3.1 Setup

Main changes in the set-up in comparison with the previous measurements are described in this section. Incident photon rate was reduced by the introduction of a Ni filter. This also eliminated to a large extent the Cu K_β line from the spectrum. A larger collimator of 8.8 mm diameter was used to compensate for the reduced rate per GEM hole by enhancing the overall flux to maintain a significant measured current. Details of the settings employed in this measurement can be seen in table 5.2.

Settings in the lab-view interface for the time intervals between consecutively recorded measurements were adjusted. The time interval was reduced from 2 s to 0.1 s.

6.3.2 Observation

Fig. 6.8 shows a comparison of the gain behavior over time for the high and low incident photon rates per GEM hole at a high voltage. This illustrates clearly that the initial rise in gain can be observed even for a high voltage effectively supporting the charge-up model.

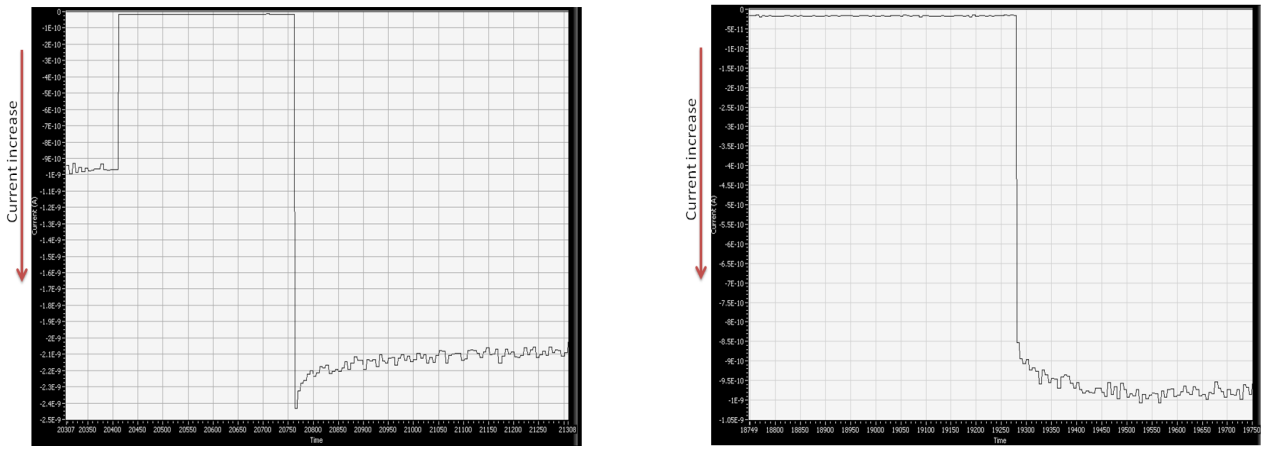

Figure 6.8: Comparison of the current vs time curve at 500 V for incident photon rates which are high (left) and low (right)
Currents plotted are negative hence an increase corresponds to going down.

The gain measurements for this setting were performed in two sets each with a different incident photon rate. The details of these settings are listed in table 5.4.

6.3.3 Real GEM gain

Gain measured on previous instances is very likely a value affected by charging up. However, by slowing down the charging up process and measuring the gain at the initial instant, GEM gain has been measured before any charging up influences affect it as seen in fig 6.11. This has been termed as 'Real gain' and is ideal for simulations which do not take charging up effects into consideration.

It has been found through simulation that a higher penning parameter results in a steeper gain curve. From fig 4.7 it can be observed that the simulated gain curves get increasingly steeper with the increase in r_{P}. In the gain curves measured previously, the values are very likely affected by charging up as was seen with earlier measurements. In accordance to the charging up model developed the following occurs- The gain measured at lower voltages is likely to be higher due to the initial rise in gain that would have occurred by the instance of measurement. Gain measured at higher voltages tends to be lower since there is a decrease in gain would have occurred by the instance of measurement due to the gain drop seen in higher voltages. As a result of this occurrence, the resulting gain curve will be less steeper than a real gain curve. Due to the perceived increase in the steepness of the gain curve an increase in penning parameter is expected. This can be seen in the increase in penning parameter estimated using the original gain curve($r_{\mathrm{P}} = 0.5$) and through the real gain curve($r_{\mathrm{P}} = 0.7$).

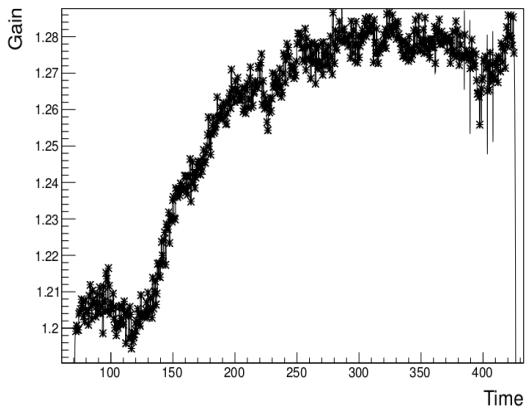

(a) $\Delta V_{\mathrm{GEM}} = 200$ V

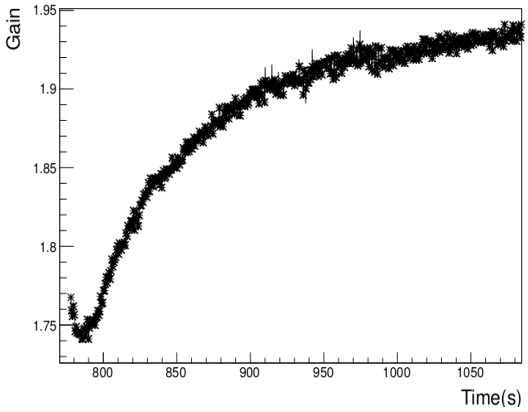

(b) $\Delta V_{\mathrm{GEM}} = 220$ V

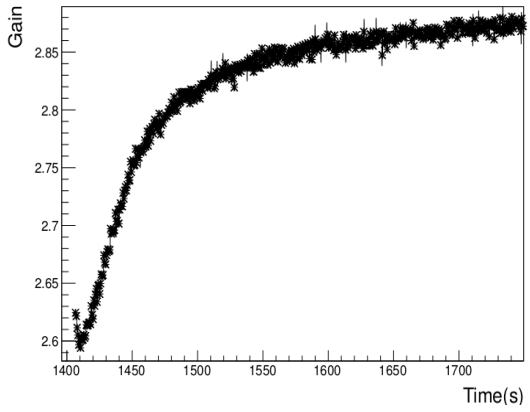

(c) $\Delta V_{\mathrm{GEM}} = 240$ V

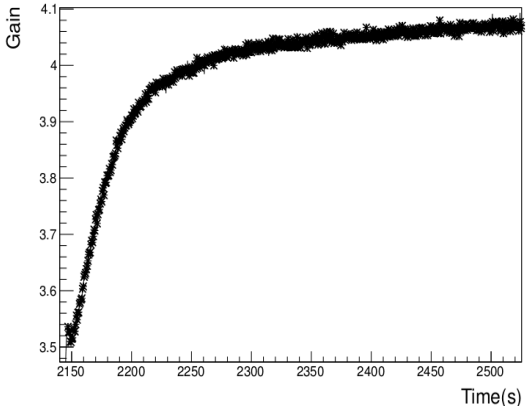

(d) $\Delta V_{\mathrm{GEM}} = 260$ V

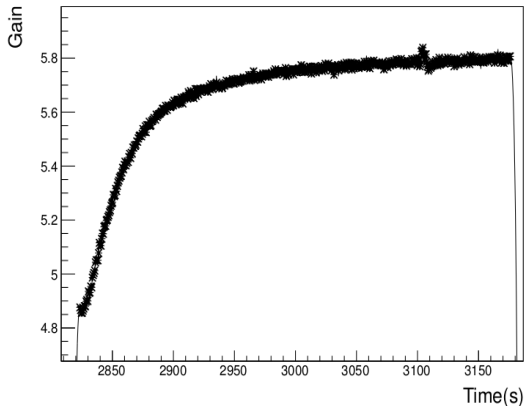

(e) $\Delta V_{\mathrm{GEM}} = 280$ V

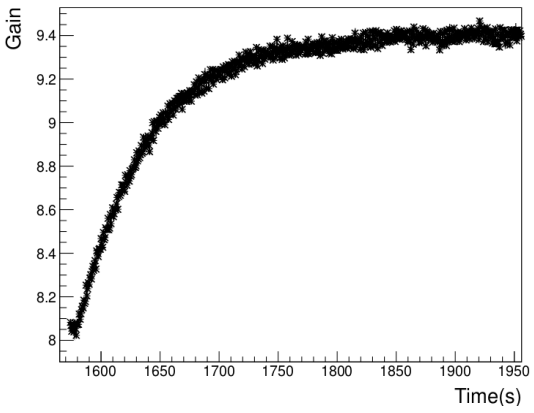

(f) $\Delta V_{\mathrm{GEM}} = 300$ V

Figure 6.9: Gain variation over time at different voltages pertinent to December low rate measurement C.1 for $\mathrm{Ar} - \mathrm{CO_2} - 70/30\%$

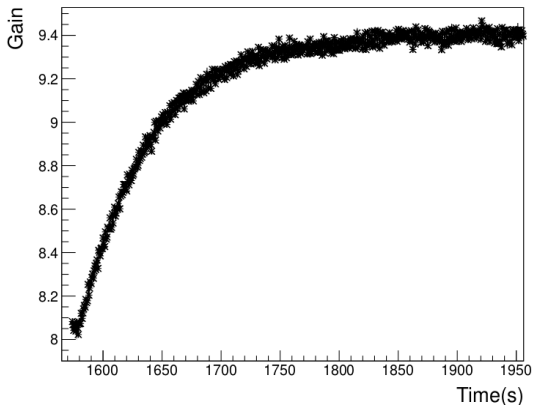

(a) $\Delta V_{\mathrm{GEM}} = 300$ V

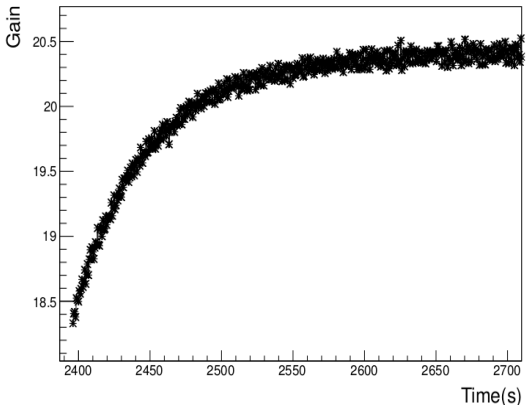

(b) $\Delta V_{\mathrm{GEM}} = 340$ V

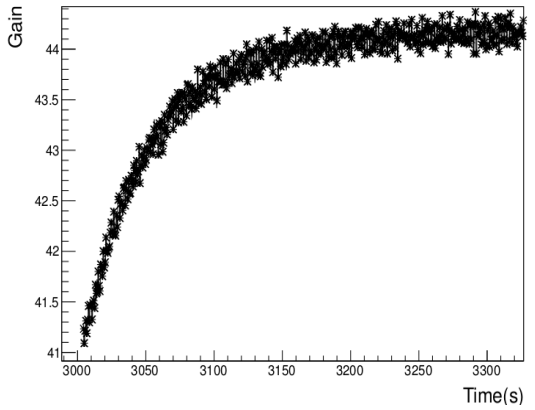

(c) $\Delta V_{\mathrm{GEM}} = 380$ V

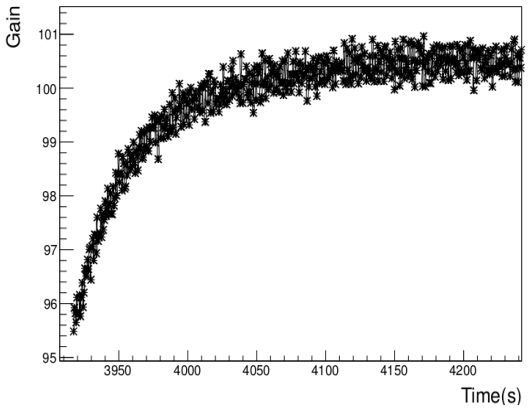

(d) $\Delta V_{\mathrm{GEM}} = 420$ V

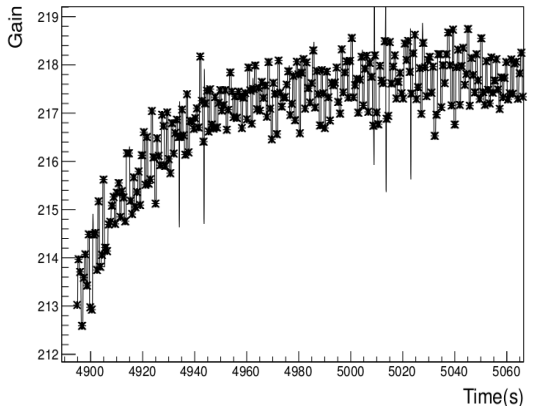

(e) $\Delta V_{\mathrm{GEM}} = 460$ V

Figure 6.10: Gain variation over time at different voltages pertinent to December low rate measurement C.2 for $\mathrm{Ar} - \mathrm{CO}_2 - 70/30\%$

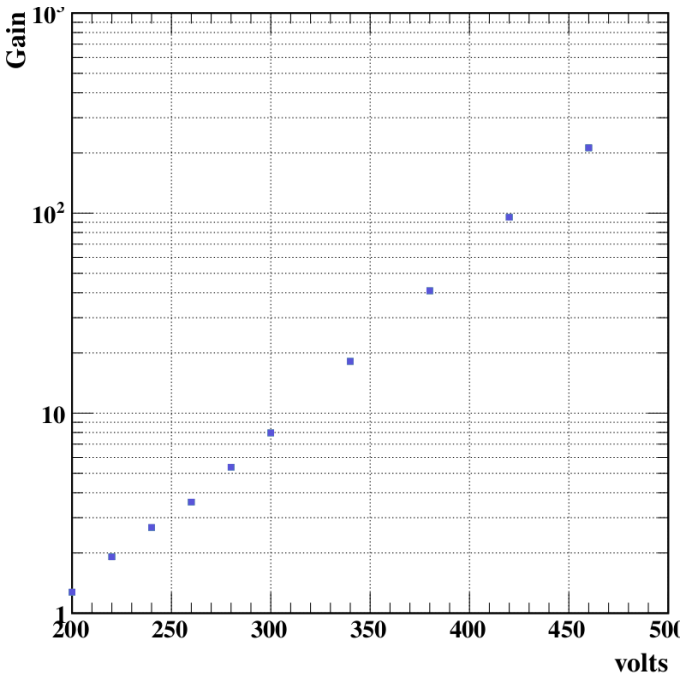

Figure 6.11: GEM gain free of charge-up effects for a $Ar - CO_2 - 70/30\%$.

6.4 Conductivity of Polyimide

In order to fully understand the charge-up process in the GEM, an understanding of the conduction mechanism through the polyimide foil used in a GEM is essential. During the normal operation of a GEM amplification generates charge carriers both electrons and ions some of which are deposited on the inner surface of the GEM holes. The amount of time taken by these carriers to reach the electrodes depends on the mobility in the medium in addition to the applied field. The chemical structure and properties of PMD as available through literature serves as a vital resource in building our understanding. GEM resistance was measured and its variation over time offers further insights into the conductivity mechanism.

6.4.1 PMD chemistry

Polyimide used in CERN standard GEMs is manufactured by the company Kaneka Texas Corporation under the name Apical® grade 200NP polyimide film. The specific variety of polyimide used in GEMs is PMDA-ODA.

The chemical structure and synthesis of Polyimide, poly-4,4-oxidiphenylene-pyromellitimide is shown in the fig 6.12.

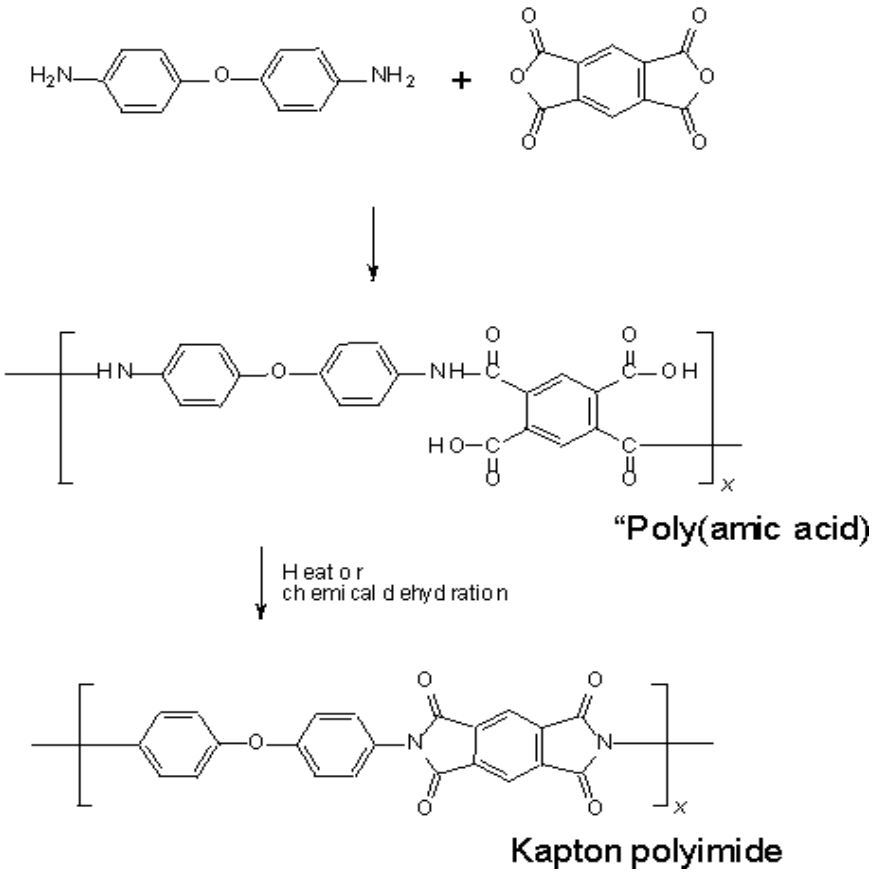

Figure 6.12: Chemical synthesis of polyimide [33]

Polyimides are synthesized from reactions between dianhydrides and diamines. The two ingredients used in this preparation are pyromellitic dianhydride also called PMDA and 4,4-oxydianiline also called ODA. PMDA has carbonyl groups which are electro-positive and hence attract electrons. ODA group has nitrogen that supplies electron. This reaction results in an intermediate compound namely polyamic acid. This group has carboxyl radicals making it acidic. Being an acid, it supplies protons in the process.

However when adequate heat is supplied, the ring is restructured while a water molecule escapes in the process. Depending on the temperature and its evenness in the baking process, residual polyamic acid and water can be found in the final polyimide synthesized. The presence of these compounds aids electrical conductivity. Charge transfer complex(CTC)

interactions between dianhydride and diamine groups results in a strong inter chain attraction which gives strength and rigidity to polyimides.

6.4.2 Literature

Charge deposition on the polyimide surfaces exposed in the GEM hole causes the alteration of electric field applied. This as discussed in the earlier sections causes the gain to vary. It is hence essential to understand the time required to evacuate the deposited charges and the mechanism through which it happens. The transit times depend on the mobility of polyimide. Charge carriers drift in a medium with a carrier mobility which is defined as the ratio of the applied electric field to the drift velocity acquired shown through the eq 6.1.

$$v_{\mathrm{d}} = \mu E \tag{6.1}$$

PMD mobility is extremely vulnerable to changes in humidity, temperature, applied electric field etc. The value of mobility remains a constant at lower electric fields and depends directly on electric field at higher values. There is a large variation in the values cited in literature. Aragoneses et al., report a mean mobility value of 2.06×10^{-13} $\mathrm{cm^2V^{-1}s^{-1}}$ for electrons and 2.37×10^{-13} $\mathrm{cm^2V^{-1}s^{-1}}$ for holes at an applied field of $E = 193$ $\mathrm{kV.cm^{-1}}$ for Kapton® type HN at $22-25^{\mathrm{o}}\mathrm{C}$ and $40-50\%$ RH (relative humidity) [34]. Sessler et al., have reported a value of 4×10^{-12} $\mathrm{cm^2V^{-1}s^{-1}}$ and 10^{-9} $\mathrm{cm^2V^{-1}s^{-1}}$ at $50^{\mathrm{o}}\mathrm{C}$ and $200^{\mathrm{o}}\mathrm{C}$ respectively [36]. Ziari et al., report a value of $0.9-1.2\times10^{-12}$ $\mathrm{cm^2V^{-1}s^{-1}}$ and $2.5-2.6\times10^{-12}$ $\mathrm{cm^2V^{-1}s^{-1}}$ at $E = 80 - 160$ $\mathrm{kV.cm^{-1}}$ and $35 - 40\%$RH [37].

Polyimide conductivity is affected by radiation dosage. Ries et al., have measured an increase in Kapton® conductivity from $4 \pm 3 \times 10^{-17}$ $\Omega^{-1}\mathrm{cm^{-1}}$ for an applied radiation of electrons at the rate of 1.0 MeV(dose rate of 5×10^4 $\mathrm{Gyh^{-1}}$) over a period of 0.5 h [38]. The sample was subject to a cumulative dosage of 9.5×10^7Gy and has been found to revert to the original un-irradiated conductivity after a period of three months. Increase in

conductivity has been attributed to the production of radicals due to the structural changes in the polymer resulting from the radiation interaction. Electron paramagnetic resonance(EPR) spectra revealed the presence of ketone , phenyl and phenoxyl radicals. Cases of non reversal of conductivity after radiation have also been reported. In the measurements made on GEM, the radiation doses are comparatively lesser and hence the radiation effects on conductivity were found to be negligible [30].

6.4.3 Experimental setup

Measurement of the resistivity of polyimide is performed by applying a high voltage across the GEM electrodes and measuring the current. At a given voltage, the current is expected to change over time.

Initial setup The experimental setup commonly used in the research group to test freshly prepared GEM foils' functioning under HV is seen in fig. 6.13. Virgin GEM foil is tested

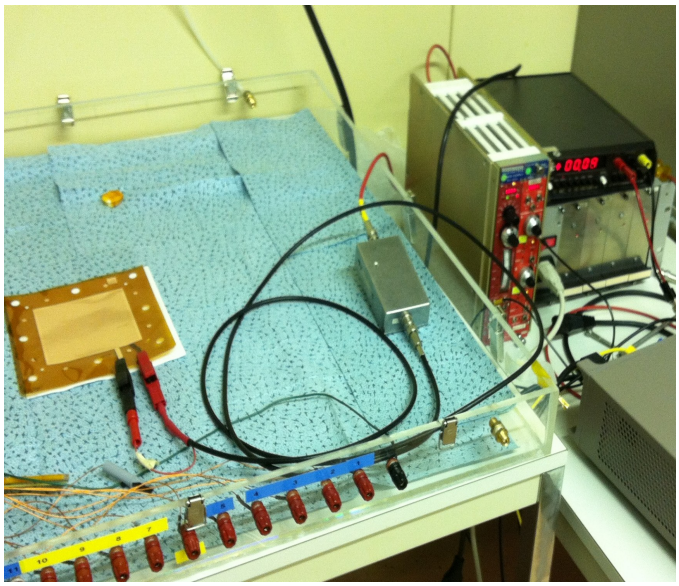

Figure 6.13: High voltage testing of a GEM foil

inside the clean room. Top and bottom electrodes of the GEM are connected to a HV supply

and the current is measured for different voltages applied. A high resistance (100 MΩ) is connected to protect the voltage supply in the event of short circuit. This method enables us to identify GEMs with possible leakages of currents greater than nano-Amperes due to manufacturing defects. Current variations of the order pico-Amperes cannot be reliably measured with this setup due to the following problems-

- Sensitivity of resistivity to humidity
- Lack of a Faraday cage to protect the circuit from external noise.

High resistance measurement setup Through this technique it was attempted to compensate for the above mentioned effects. GEM foil was placed inside the timing GEM chamber under circulation of a 100% CO_2 for three weeks. This ensured that the foil was devoid of humidity. The foil was previously unused for one month since a gain measurement performed in December2012. The chamber was mounted inside a Faraday as shown in the fig. 5.2 earlier. Connections were made according to the description in the Keithley manual for the electro-meter 6517 as shown in the fig. 6.14. Both the electrodes of GEM were connected to

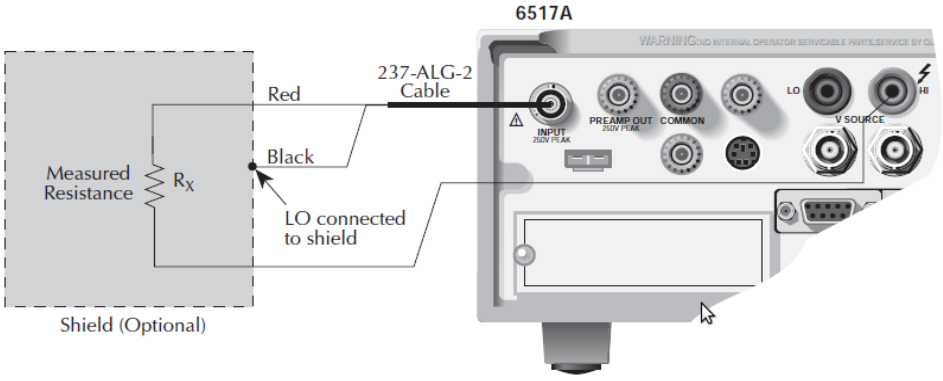

Figure 6.14: High resistance measurement technique as depicted in the manual of Keithley electro-meter 6517A [39]

the electro-meter 6517 which supplied a voltage set to 500 V and the current was measured by the same instrument. Values of current were recorded over time. After leaving the GEM under HV for 24 hours, the voltage on 6517 was set to 0 V effectively shorting the GEM

terminals. The current was later recorded as a function of time.

6.4.4 Observation

Measured current varied over time and exhibited a behavior shown in the fig. 6.15(left). The current behavior over time was not constant like a resistor, nor was it exponential like a capacitor. It was also not linear. The dependence followed a $\frac{1}{t}$ rule as seen from the fit to the measured data. A similar behavior was observed even in the decay part of the curve.

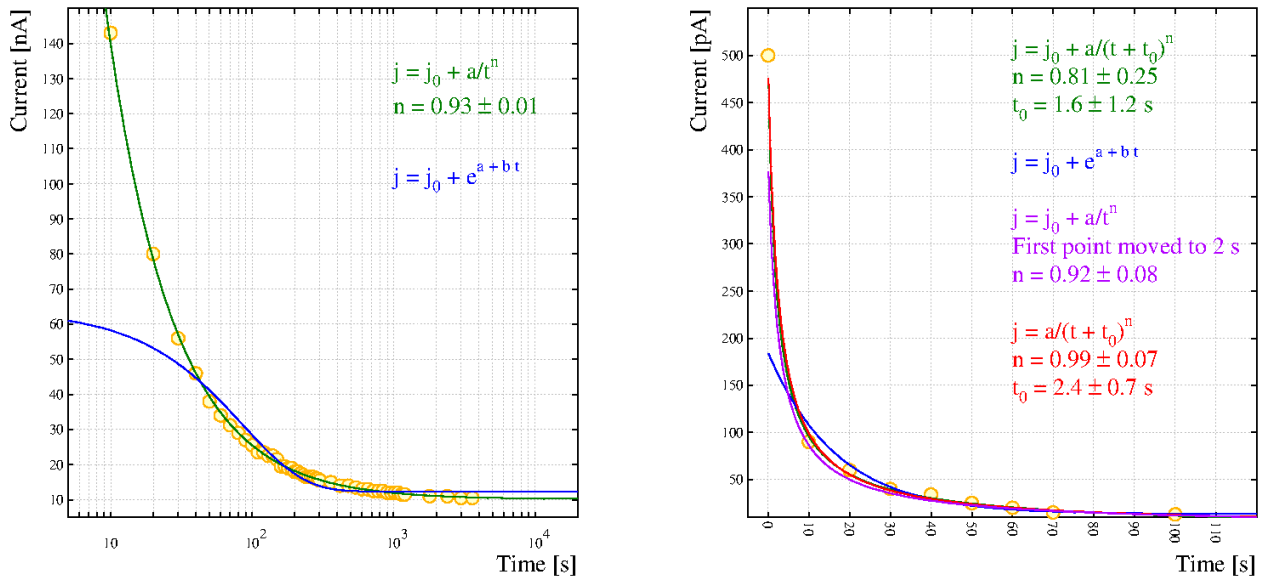

Figure 6.15: Left: Variation of current over time in a GEM under high voltage. Right: Subsequent variation of current over time in a shorted GEM

Analysis The observed decay of current seemed to follow the Kohlrausch's relaxation process. A detailed account of the processes and the physics involved can be found in the [40]. There are many physical models that suit the relaxations but one particular model is relevant to our scenario. Let us consider a polymer substance under the influence of electric field applied on either ends through electrodes. Ions and free radicals in the polymer move under the influence of the applied field. This motion causes a current which can be measured. At the electrode polymer interface a thin oxide layer with thickness of the order of 0.1 nm gets developed. Although the layer does not prevent the motion of electrons across itself,

ions and radicals cannot cross the thick layer. Presence of metal electrode adjacent to the oxide layer gives rise to a mirror effect where oncoming charges see their images across the oxide layer. This causes an electrostatic attraction which enhances the motion of the charges moving towards the electrode and also brings a deviation from a constant current. The above described phenomenon gives rise to the observed $\frac{1}{t}$ dependence.

The chemical structure of polyimide is such that they form a type of bonding. Presence of water molecules usually causes the H+ and OH- groups to separate and the protons cause conduction. This is dominant initially and goes down gradually with time going upto hours to decrease an order of magnitude. In our case, the GEM is sufficiently clean and dry hence the possibility of moisture induced conduction is ruled out. This is one reason why very high resistivity is noted in our samples. The rapid decay in the current still needs to be explained.

This observation has an important consequence in the understanding of charge conduction process in PMD. It can be concluded that the conduction is due to ions and radicals since they will not be able to cross the oxide layer at the electrode-polymer interface and hence get accumulated resulting in a decay of the current.

6.4.5 Results

Steady state resistivity of the PMD has been found to be around 10^{18} Ωcm at $E = 100\,\mathrm{kV.cm^{-1}}$. The high measured value can be a consequence of the extremely dry sample and the presence of $Cu - Cr$ electrode.

Fig 6.16(right) shows the comparison of steady state resistivity with the values measured by E.Motyl at 100 $kVcm^{-1}$ [41], E.Motyl and R.Kacprzyk at 20 $\mathrm{kVcm^{-1}}$ [42] both for a 25 μm thick Kapton® HN with Al electrodes, in addition to other sources mentioned before.

There are two components of the current, the transient and the steady state. Transient current is the result of the flow of protons, ions and other radicals. This current decreases over time since there is a finite supply of these carriers in the polymer. Steady state current is due to the flow of electrons and extremely slow moving ions and radicals that contribute

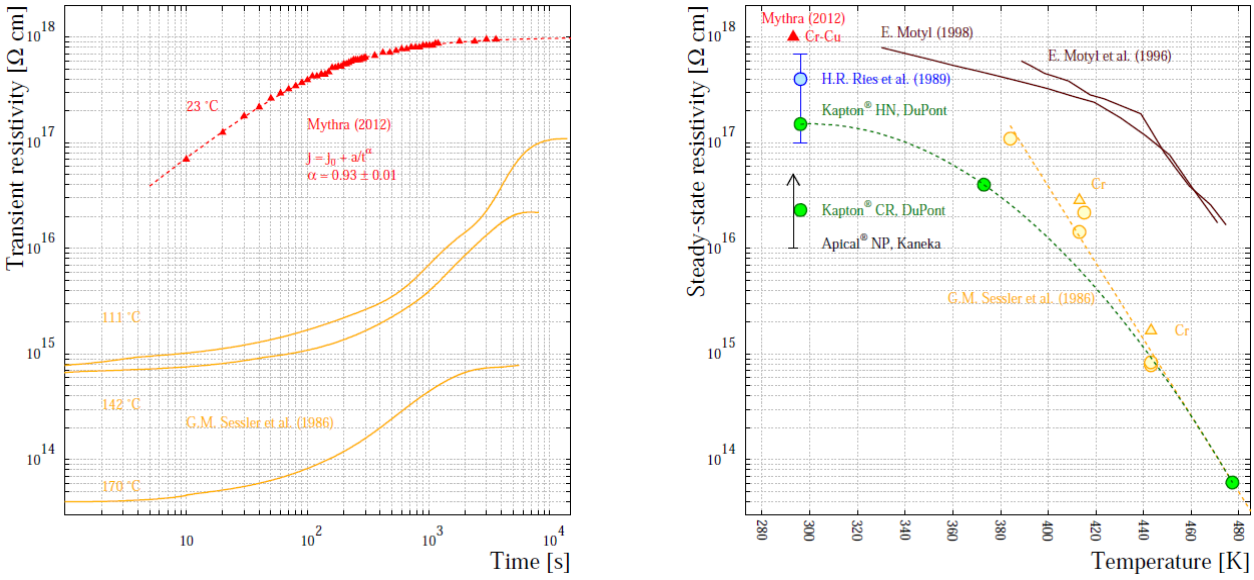

Figure 6.16: Left: Transient resistivity increasing and stabilizing towards a steady value, Right: Measured steady state resistivity in comparison with values from literature at various temperatures.

to a smaller current.

The transit times of the charge carriers through PMD at the given resistivity can be seen in fig 6.17(right). Transit time is the time required by the charge deposited to travel through the bulk to reach the electrode. It can be estimated that on application of electric field charge evacuation on a GEM is possible in timescales of the order or hours(10^4 s) to days(10^5 s). The transit times for both electrons and positive ions is comparable given the uncertainty in the mobility measurement.

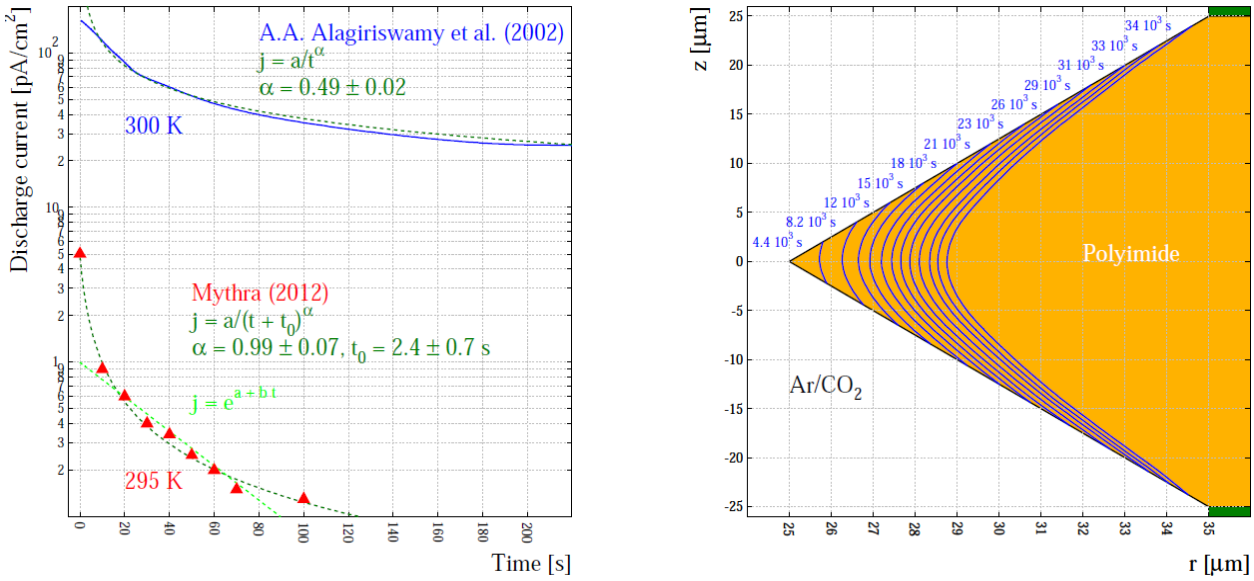

Figure 6.17: Left: Measured discharging current in comparison with the measurement of A.A. Alagiriswamy et al.(2002), Right: Transit times of the charge carriers inside polyimide. A section of GEM hole is seen with marked trajectories of the charges.

7 CONCLUSIONS AND FUTURE WORK

A full understanding of the Gas Electron Multiplier working has been achieved through simulations and other experiments for the first time. The gain has been computed through simulation which is nearly half the measured value, this is an improvement over previous comparisons with simulations which were a factor of 6 lower than measurements as shown by Croci [24].

The discrepancy is still being studied. GEM gain free of charging up effects has been measured through experiments that have been performed at a lowered rate of incident radiation per GEM hole. Gain has been found to be affected by less than 10% due to charging up as found through simulations. Charging up simulations have been performed by R.Veenhof and P.Correia and the comparisons were consistent with the measurements and have observed that the variation in field does stabilize over time due to the charge compensation of ions and electrons.

Simulations on the dependence of gain on hole diameter have revealed an optimal value without indications of stable plateau region as indicated by prior measurements. To experimentally verify this result, GEMs with various hole diameters ranging from 30 μm to 120 μm have been fabricated. These measurements in future can offer a solution to the problem of robustness of gain behavior in spite of the inconsistencies in the hole size due to fabrication limitations.

Although the charging up effects on a single GEM were studied and characterized in this work, it is not a reflection of the mechanisms involved in a triple GEM. Triple GEMs have been shown to have a far greater gain stability presumably due to a more complicated mechanism involved as a result of multiple stages.

Experiments on polyimide conductivity show a greater likelihood of bulk conduction as against surface conduction. The physics involved in charge transport has been understood. A steady state resistivity of 10^{18} Ω has been measured and a possible mechanism for the evacuation of charges deposited on the polyimide has been found.

Building on this work, research directed to understand triple GEMs and other kinds of GEMs can be undertaken in future. These studies will play a key role to better harness the potential of GEMs which are being applied to a wide range of areas today.

Bibliography

[1] S. Dildick; P. Corriea; A. Mohapatra; T. Moulik; M. Nemallapudi and R. Veenhof, Understanding the gas gain in GEM detectors (to be published)

[2] F. Sauli, GEM: a new concept for electron amplification in gas detectors, Nucl. Instr. and Meth. in Physics Research A 386 (1997) 531

[3] The Super-LHC is on the starting blocks, CERN courier, Jul-8-2008

[4] A. Sharma, Nuclear Instruments and Methods in Physics Research A 666(2012)98129

[5] CMS Internal Note, A GEM Detector System for an Upgrade of the CMS Muon Endcaps, submitted Feb-10, 2012

[6] H. Bethe and J. Ashkin in Experimental Nuclear Physics, ed. E. Segré, J. Wiley, New York, 1953, p. 253

[7] U.Fano, Ionization Yield of Radiations. II. The Fluctuations of the Number of Ions, Physical Review 72 (1), Jul-01-1947

[8] F. Sauli, Principles of operation of Multi Wire Proportional Chambers and Drift Chambers, CERN 77-09, 03-May-1977

[9] Hünteler, Henning. Development and Evaluation of a Multiwire Proportional Chamber for a High Resolution Small Animal PET Scanner - Westfalische Wilhelms-Universitat Munster Institut fur Kernphysik, Feb 2007

[10] G. Charpak; R. Bouchlier; T. Bressani; J. Favier and C. Zupancic, Nucl. Instrum. Methods 62, 235 (1968).

[11] Spieler,Helmuth. XII-Gaseous detectors - Introduction to Radiation detection and Electronics, 27-Apr-1999

[12] Serge Duarte Pinto, Gas Electron Multipliers: Development of large area GEMs and spherical GEMs, UNIVERSITAT BONN Physikalisches Institut

[13] A.Sharma et al., Construction and Performance of Large-Area Triple-GEM Prototypes for Future Upgrades of the CMS Forward Muon System, RD51-Note-2011-012, arXiv:1111.7249v1 [physics.ins-det] 30 Nov 2011

[14] S. Bachmann; A. Bressan; L. Ropelewski; F. Sauli; A. Sharma and D. Mrmann, "Charge amplification and transfer processes in the gas electron multiplier" - CERN-EP/99-48, 1999

[15] J.Rice (1995). Mathematical Statistics and Data Analysis (Second ed.). Duxbury Press. ISBN 0-534-20934-3.

[16] M.J. Druyvesteyn and F.M. Penning, The Mechanism of Electrical Discharges in Gases of Low Pressure, Rev. Mod. Phys. 12 (1940) 87 [Erratum ibid. 13 (1941) 72].

[17] Ö. Şahin, İ. Tapan, E.N. Özmutlu and R. Veenhof, Penning transfer in argon-based gas mixtures, JINST- 5 P05002, 04-May-2010

[18] A Laboratory Manual for X-Ray Powder Diffraction, U. S. Geological Survey Open-File Report 01-041, http://pubs.usgs.gov/of/2001/of01-041/htmldocs/xrpd.htm

[19] XRF analysis, SII Nanotechnology Inc., http://www.siint.com

[20] ANSYS Inc., ANSYS version 11 Electromagnetics, 2010

[21] S.Biagi, Magboltz- transport of electrons in gas mixtures, http://consult.cern.ch/writeups/magboltz/. 31, 35, 38

[22] R. Veenhof, Garfield - simulation of gaseous detectors, http://garfield.web.cern.ch/garfield/

[23] S. Dildick,"Avalanche Simulations on single GEMs", MPGD meeting -68, CERN

[24] G. Croci, "Development and Characterization of Micro-Pattern Gaseous Detectors for HEP applications and beyond," University of Siena, Faculty of Mathematical, Physical and Natural Sciences, Department of Physics, Ph.D thesis in Experimental Physics, XXIII Cycle (2011)

[25] L. Franconi, Performance of large-size triple GEM detectors for the CMS Forward Muon Upgrade project, UNIVERSITA DI BOLOGNA, Mar-2012

[26] http://www.amptek.com/software.html

[27] A.C. Thompson et al., Xray data booklet, edited by A.C. Thompson and D. Vaughan , Lawrence Berkeley National Laboratory, Berkeley, CA, USA (2009).

[28] G. Castellano; J. Osán and J. Trincavelli, Analytical model for the bremsstrahlung spectrum in the $0.25-20\ keV$ photon energy range, Spectrochimica Acta Part B: Atomic Spectroscopy 59 (2004) 313-319.

[29] Private communication with PANalytical Xray tube manufacturing company

[30] Diploma of G. Croci

[31] T. Tamagawa; N. Tsunoda; A. Hayato; H. Hamagaki; M. Inuzuka; H. Miyasaka; I. Sakurai; F. Tokanai and K. Makishima, Development of gas electron multiplier foils with a laser etching technique, Nuclear Instruments and Methods in Physics Research A 560 (2006) 418-424

[32] J. Benlloch; A. Bressan; M. Capeáns; M. Gruẃe; M. Hoch; J.C. Labbé; A. Placci; L. Ropelewski and F. Sauli, Further developments and beam tests of the gas electron multiplier (GEM), Nuclear Instruments and Methods in Physics Research A 419 (1998) 410-417

[33] http://chem.chem.rochester.edu/ chem421/errata.htm

[34] Aragoneses; M. Mudarra; J. Belana and J.A. Diego, Study of dispersive mobility in polyimide by surface voltage decay measurements, Polymer 49(2008) 2440-2443.

[35] A.A. Alagiriswamy; K.S. Narayan and Govinda Raju, Relaxation processes in aromatic polyimide, Journal of Physics D: Applied Physics 35 (2002) 2850-2856.

[36] G.M.Sessler; B. Hahn and D.Y. Yoon, Electrical conduction in polyimide films, Journal of Applied Physics 60(1986) 318-326.

[37] Z. Ziari; S. Sahli; A. Bellel; Y. Segui and P. Raynaud, Simulation of surface potential decay of corona charged polyimide, IEEE Transactions on Dielectrics and Electrical Insulation 18 (2011) 14081415.

[38] H.R.Ries; W.L. Harries; S.A.T. Long and E.R. Long, Jr, , Mechanism of electrical conductivity in irradiated polyimide, Journal of Physics and Chemistry of Solids 50(1989) 735-738

[39] Manual for Keithley electrometer 6517

[40] H.Kliem, Kohlrausch relaxations: new aspects about the everlasting story, IEEE transactions on Dielectrics and Electrical Insulation 12(2005) 709-718

[41] E.Motyl, Electrode effects and electrical conduction in polyimide kapton HN films, International Conference on Conduction and Breakdown in Solid Dielectrics(ICSD 98), 237-240, 1998.

[42] E.Motyl and R.Kacprzyk, On the electrical conduction in polyimide, 9th International Symposium on Electrets (ISE 9), 608-613, 1996.